RADC-TR-90-319
Final Technical Report
December 1990

ANTENNA AND BACKSCATTERING PATTERNS OF REFLECTORS THAT ARE PARTIALLY RESISTIVE

USAF Academy

Randy L. Haupt, Major, USAF

Rome Air Development Center
Air Force Systems Command
Griffiss Air Force Base, NY 13441-5700

This report has been reviewed by the RADC Public Affairs Division (PA) and is releasable to the National Technical Information Service (NTIS). At NTIS it will be releasable to the general public, including foreign nations.

RADC-TR-90-319 has been reviewed and is approved for publication.

APPROVED: Marc G. Coté

MARC G. COTE
Project Engineer

APPROVED: John K Schindler

JOHN K. SCHINDLER
Director of Electromagnetics

FOR THE COMMANDER: Igor G. Plonisch

IGOR G. PLONISCH
Directorate of Plans & Programs

If your address has changed or if you wish to be removed from the RADC mailing list, or if the addressee is no longer employed by your organization, please notify RADC (EECT) Hanscom AFB MA 01731-5000. This will assist us in maintaining a current mailing list.

Do not return copies of this report unless contractual obligations or notices on a specific document require that it be returned.

REPORT DOCUMENTATION PAGE

Form Approved
OMB No. 0704-0188

1. AGENCY USE ONLY (Leave Blank)	2. REPORT DATE	3. REPORT TYPE AND DATES COVERED
	December 1990	Final Jan 89 to May 89

4. TITLE AND SUBTITLE
ANTENNA AND BACKSCATTERING PATTERNS OF REFLECTORS THAT ARE PARTIALLY RESISTIVE

5. FUNDING NUMBERS
C - P.O. #95670012
PE - 61102F
PR - 2305
TA - J4
WU - P6

6. AUTHOR(S)
Randy L. Haupt, Major, USAF

7. PERFORMING ORGANIZATION NAME(S) AND ADDRESS(ES)
USAF Academy
Colorado Springs CO 80840-5017

8. PERFORMING ORGANIZATION REPORT NUMBER
N/A

9. SPONSORING/MONITORING AGENCY NAME(S) AND ADDRESS(ES)
Rome Air Development Center (EECT)
Hanscom AFB MA 01731-5000

10. SPONSORING/MONITORING AGENCY REPORT NUMBER
RADC-TR-90-319

11. SUPPLEMENTARY NOTES
RADC Project Engineer: Marc C. Cote/EECT/(617) 377-4267

12a. DISTRIBUTION/AVAILABILITY STATEMENT
Approved for public release; distribution unlimited.

12b. DISTRIBUTION CODE

13. ABSTRACT (Maximum 200 words)

This report examines the backscattering patterns and far field radiation patterns of two-dimensional corner reflector and parabolic reflector antennas for E-polarization. A surface integral equation formulation is employed to obtain the current density on a resistive reflector surface. The current is then integrated to obtain the radar cross section and far field receive radiation pattern. The same method is then used to calculate the scattering and radiation patterns of corner and parabolic reflector antennas with resistive surfaces. This analysis demonstrates that, when the entire reflector is resistive (rather than conducting) a reduction of the large backscattering lobes for front and back broadside incidence occurs along with a substantial reduction in gain. Tapering the resistivity of the surface, however, has little effect on the front and back backscattering lobes, but reduces the scattering sidelobes. The tapers significantly reduce the radiation pattern sidelobes with little reduction in gain.

14. SUBJECT TERMS	15. NUMBER OF PAGES
Antennas Reflectors Antennas RCS Reflector Scattering Tapered Reflectors Antenna Scattering Antenna Camouflage Resistive Reflectors	64
	16. PRICE CODE

17. SECURITY CLASSIFICATION OF REPORT	18. SECURITY CLASSIFICATION OF THIS PAGE	19. SECURITY CLASSIFICATION OF ABSTRACT	20. LIMITATION OF ABSTRACT
UNCLASSIFIED	UNCLASSIFIED	UNCLASSIFIED	UL

Contents

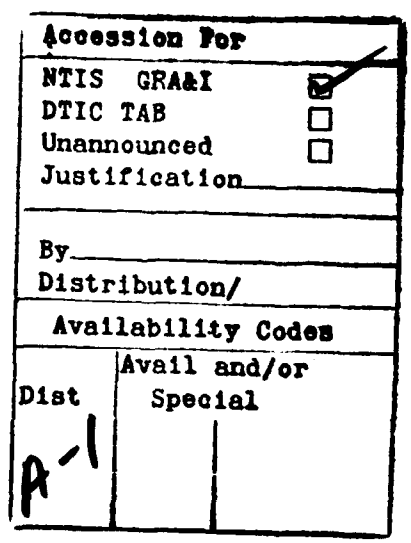

ILLUSTRATIONS

TABLE

1. INTRODUCTION

Receive antennas are apertures that collect incident electromagnetic energy. This collecting aperture consists of three parts: the effective aperture, the loss aperture, and the scattering aperture [1]. The effective aperture accounts for the incident electromagnetic energy that arrives at the load, while the loss aperture accounts for the incident electromagnetic energy converted to heat, and the scattering aperture accounts for the incident electromagnetic energy reradiated or scattered from the antenna. Maximum power transfer occurs when the antenna is lossless and the load is matched. Under these conditions, the power delivered to the load equals the power reradiated from the antenna.

On the one hand, scattering from an antenna can enhance the antenna's performance, as in the Yagi-Uda array. The Yagi-Uda array has one active element and several passive elements which only serve to reradiate incident electromagnetic radiation. When the elements of this array are properly positioned, the antenna adds the radiation from the active and passive elements to obtain a highly directional antenna pattern.

On the other hand, scattering from an antenna can degrade an antenna's performance. For instance, mutual coupling between elements must be taken into account in the design of low sidelobe antennas. Also, scattering from the edge of a ground plane causes undesirable deviations in the antenna pattern. These problems have been extensively studied and reported in the literature [2].

Antenna scattering or antenna radar cross-section (RCS) has not received much attention in the literature. Antennas are designed to achieve the best possible far field antenna pattern without considering the antenna's RCS pattern. Knowing the far field pattern of an antenna gives little indication of its RCS pattern, however. If the antenna is to have certain RCS characteristics, then the initial design must include an analysis of and trade-off between the desired far field and RCS patterns.

The goal of this research is to examine the backscattering patterns and far field radiation patterns of reflector antennas, then develop methods of re-shaping the antenna and/or varying its material composition to simultaneously obtain desirable radiation and scattering characteristics.

This first report examines the radiation and scattering characteristics of two-dimensional corner reflector and parabolic reflector antennas for E-polarization. Figure 1.1 shows a diagram of a corner reflector and its feed, while Figure 1.2 shows a diagram of a parabolic reflector and its feed. In both figures the incident electric field is E-polarized or

$$\bar{E} = \hat{z}\, E_o e^{jk\rho} \tag{1.1}$$

where

$\rho = x\cos\phi_o + y\sin\phi_o$

$k = 2\pi/\text{wavelength}$

$\phi_o =$ incident angle of plane wave

Both reflectors are two-dimensional and the parabola has a feed composed of a collection of line sources located at $(x_i^f\ ,\ y_i^f)$. The corner reflector has two sides each of width a and an angle between them of ϕ_c.

This report begins by describing the mathematical development of two-dimensional reflectors and their feeds for E-polarization. Then, the radiation and scattering characteristics of corner reflectors and parabolic reflectors are examined.

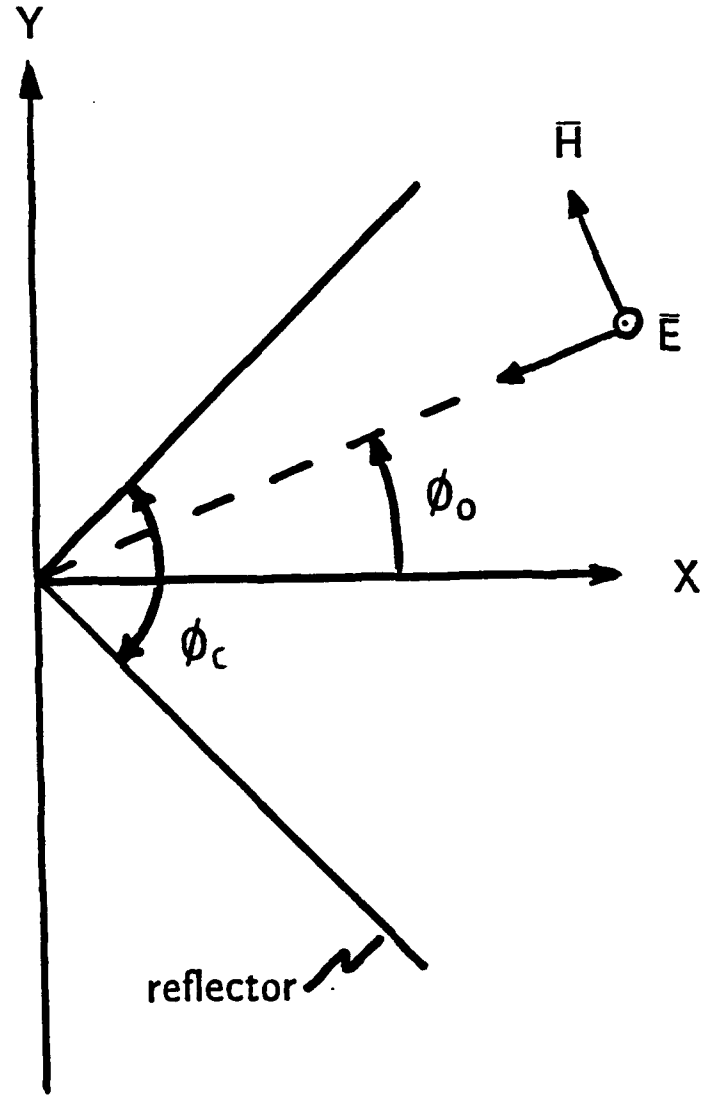

Figure 1.1 Model of a two-dimensional corner reflector with an E-polarized incident plane wave.

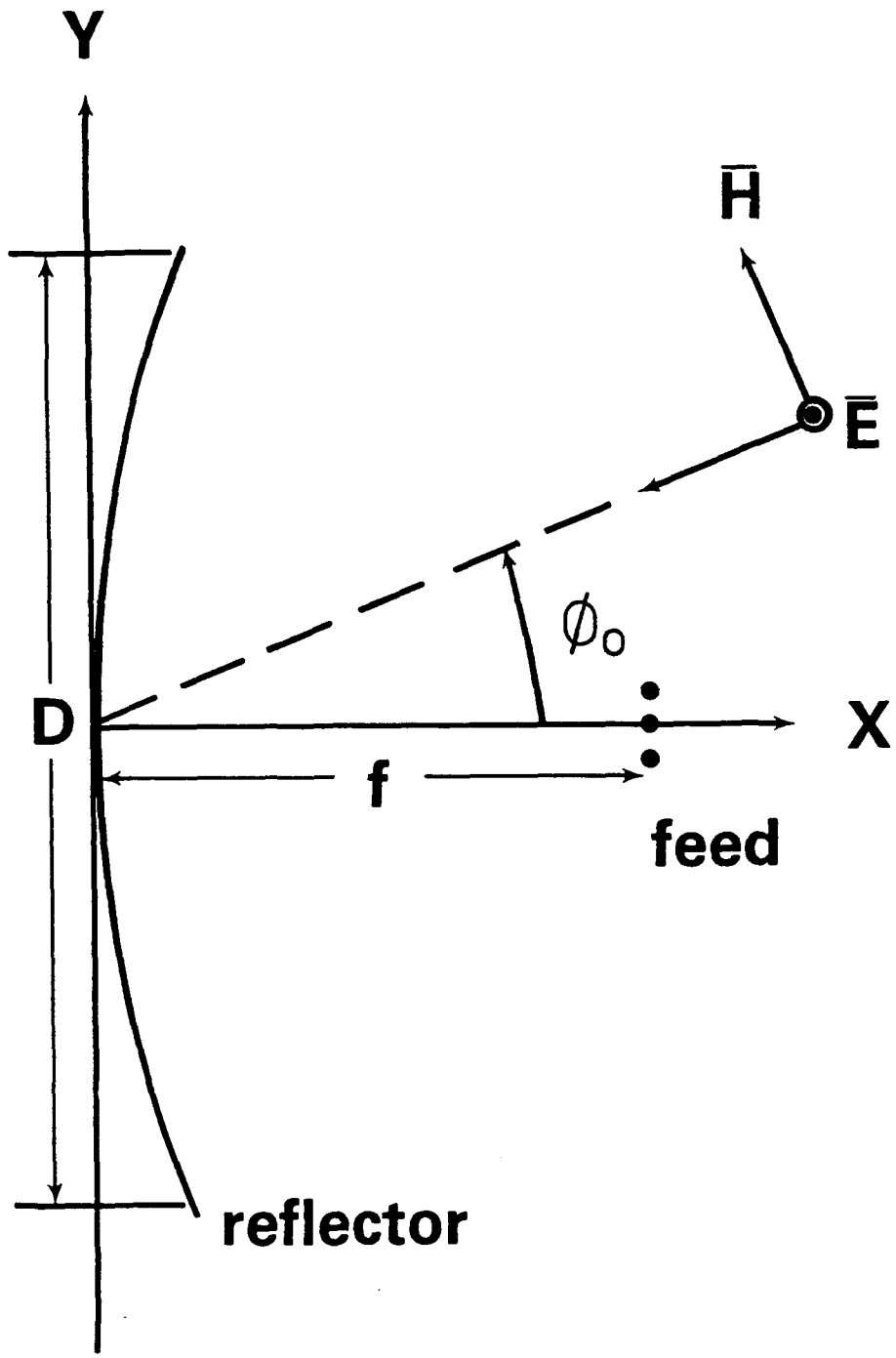

Figure 1.2 Model of a two-dimensional parabolic reflector antenna with a phased array feed at the focal point and an E-polarized incident plane wave.

2. E-POLARIZATION INTEGRAL EQUATIONS FOR TWO-DIMENSIONAL REFLECTORS

This section presents the integral equation formulation for calculating the current density on a two-dimensional reflector antenna due to an incident E-polarized plane wave. The integral equation is solved numerically for the induced surface current. Once the induced surface current is found, the RCS and the receive radiation pattern of the reflector are calculated.

2.1 Integral Equation Formulation

The total electric field equals the sum of the incident and scattered electric fields.

$$\overline{E}^T = \overline{E}^i + \overline{E}^s \tag{2.1-1}$$

Superscripts indicate total field (T), incident field (i), and scattered field (s). The incident field is given by (1-1). Since the reflector may be composed of both conducting and resistive materials, the total tangential electric field at the surface of the reflector is given by [3]

$$E^T_{tangent}(\bar{\rho}) = R(\bar{\rho})\, J_z(\bar{\rho}) \tag{2.1-2}$$

where

$\bar{\rho}$ = location of point on surface

$R(\bar{\rho})$ = resistivity variation along the surface of the reflector

$J_z(\bar{\rho})$ = z-directed surface current

The scattered field is written as

$$\overline{E}^s = -jw\overline{A} - \nabla\nabla\cdot\overline{A} \qquad (2.1\text{-}3)$$

where

$$\overline{A} = \mu_o \int_{-a}^{a} J_z(\bar{\rho}')\, G(\bar{\rho} \mid \bar{\rho}')\, d\rho'$$

μ_o = permeability of free space

$\bar{\rho}'$ = vector from origin to source point on the reflector

$\bar{\rho}$ = vector from origin to field observation point

$G(\bar{\rho} \mid \bar{\rho}')$ = Green function = $\frac{1}{4j} H_o^{(2)}(k \mid \bar{\rho} - \bar{\rho}'|)$

$H_o^{(2)}(k \mid \bar{\rho} - \bar{\rho}'|)$ = zeroth order Hankel function of the second kind

k = wave number

For E-polarization, $\nabla\cdot A_z\hat{z} = 0$ leaving

$$E^s = \frac{-\omega\mu_o}{4} \int_{-a}^{a} J_z(\bar{\rho}')\ H_o^{(2)}(k \mid \bar{\rho} - \bar{\rho}'|)\, d\bar{\rho}' \qquad (2.1\text{-}4)$$

where ω is the radial frequency.

Substituting (1-1), (2.1-2), and (2.1-4) into (2.1-1) produces

$$E_o e^{jk\rho} = R(\rho)\, J_z(\rho) + \frac{kZ_o}{4} \int_{-a}^{a} J_z(\rho')\ H_o^{(2)}(k \mid \bar{\rho} - \bar{\rho}'|)\, d\rho' \qquad (2.1\text{-}5)$$

The normalized resistivity is given by $\eta(\rho) = R(\rho)/Z_o$, where Z_o is the intrinsic impedance of free space. Substituting $\eta(\rho)$ into (2.1-5) and assuming that $E_o = Z_o$ gives

$$e^{jk\rho} = \eta(\rho)\, J_z(\rho) + \frac{k}{4} \int_{-a}^{a} J_z(\bar{\rho}')\ H_o^{(2)}(k \mid \bar{\rho} - \bar{\rho}'|)\, d\bar{\rho}' \qquad (2.1\text{-}6)$$

Solving this for the current density is the first step to finding the RCS or far field pattern.

2.2 Numerical Solution of Integral Equation

Equation (2.1-6) is solved using point matching [4]. The current density is represented by a sum of N basis functions,

$$J_s(\rho) = \sum_{n=1}^{N} \alpha_n J_n(\rho) \tag{2.2-1}$$

where

J_n = set of basis functions

α_n = weighting coefficients

Substituting (2.2-1) into (2.1-6) and matching the boundary conditions at N collocation points on the surface of the reflector produces the following set of equations:

$$e^{jk\rho_m} = \sum_{n=1}^{N} \alpha_n \left[\eta(\rho_m)\, J_n(\rho_m) + \frac{k}{4}\int_{-a}^{a} J_n(\rho')\ H_o^{(2)}(k|\bar{\rho}_m - \bar{\rho}'|)\, d\rho'\right] \tag{2.2-2}$$

for m=1,2,...,N. Putting (2.2-2) into the matrix form Ax=B yields

$$\begin{bmatrix} a_{11} & a_{12} & \cdots & a_{1N} \\ a_{21} & a_{22} & \cdots & a_{2N} \\ \vdots & \vdots & & \vdots \\ a_{N1} & a_{N2} & \cdots & a_{NN} \end{bmatrix} \begin{bmatrix} \alpha_1 \\ \alpha_2 \\ \vdots \\ \alpha_N \end{bmatrix} = \begin{bmatrix} b_1 \\ b_2 \\ \vdots \\ b_N \end{bmatrix}$$

where

$$b_m = e^{jk\rho_m}$$

$$a_{mn} = \eta(\rho_m)\, J_z(\rho_m) + \frac{k}{4}\int_{-a}^{a} J_z(\rho')\ H_o^{(2)}(k \mid \bar{\rho}_m - \bar{\rho}'|)\, d\rho'$$

Solving the matrix equation for the unknown coefficients, α_n, then substituting into (2.2-1) results in an approximation of the strip current density.

The reflector surface is divided into N segments of equal size with the collocation points at the center of each segment. If the current is expanded in pulse basis functions, then a pulse exists only over one of these segments and is represented by

$$J_n(x_m) = \begin{cases} 1, & |x_m - x_n| < \frac{\Delta}{2} \\ 0, & \text{otherwise} \end{cases}$$

where $\Delta = x_{m+1} - x_m$. Substituting the pulses into (2.2-3) results in

$$e^{jk\rho_m} = \sum_{n=1}^{N} \alpha_n \left[\delta_{mn}\eta(\rho_m)\, J_n(\rho_m) + \frac{k}{4}\int_{-a+(n-1)\Delta}^{-a+n\Delta} H_o^{(2)}(k|\bar{\rho}_m - \bar{\rho}'|)\, d\bar{\rho}' \right] \qquad (2.2\text{-}3)$$

for m=1,2,...,N and where

$$\delta_{mn} = \begin{cases} 1, & m=n \\ 0, & \text{otherwise} \end{cases}$$

The integral in (2.2-3) is straightforward to evaluate except at $\rho=\rho'$. At this point the Hankel function has a weak (logarithmic) singularity that requires a special integration procedure.

Midpoint integration is a simple yet accurate integration technique if the integration points are about $\frac{\lambda}{10}$ apart on the strip. The midpoint integration formulas for the matrix elements are given by

$$a_{mm} = \eta(\rho_m) + \frac{k}{4}\Delta[1 - j\tfrac{2}{\pi}(0.0287983 + \ln\Delta)] \qquad m=n \qquad (2.2\text{-}5)$$

$$a_{mn} = \frac{k}{4}\Delta H_o^{(2)}(k|\bar{\rho}-\bar{\rho}'|) \qquad m\neq n \qquad (2.2\text{-}6)$$

2.3 Radar Cross-Section Evaluation

The electric field scattered by the reflector is given by (2.1-4). In the far field ($\rho \gg \rho'$), the Hankel function may be replaced by its large argument approximation [5].

$$H_o^{(2)}(k|\bar{\rho}_m - \bar{\rho}'|) \simeq \frac{e^{j(\frac{\pi}{4} + k|\bar{\rho}_m - \bar{\rho}'|)}}{\sqrt{.5\pi k|\bar{\rho}_m - \bar{\rho}'|}} \tag{2.3-1}$$

A two-dimensional bistatic RCS is calculated from

$$\sigma(\phi) = \lim_{\rho \to \infty} 2\pi\rho \left| \frac{E^s(\phi)}{E^i(\phi_o)} \right|^2 \tag{2.3-2}$$

which for E-polarization is

$$\sigma_E(\phi) = \frac{k}{4} \left| \int_{-a}^{a} J_z(\rho') e^{jk\rho'} d\rho' \right|^2 \tag{2.2-3}$$

Backscattering RCS assumes $\phi = \phi_o$ in these equations. The RCS can be normalized to the wavelength, so RCS = $\sigma_E(\phi)/\lambda$. Thus, rather than expressing the RCS in terms of dBm (decibels relative to a meter), the RCS is in units of $dB\lambda$.

2.4 Receive Pattern Evaluation

The receive pattern is calculated by summing all the electric fields incident on each feed element, multiplying the sum by the corresponding element pattern and weight, then summing the outputs from all the feed elements. Both the incident and scattered fields must be added appropriately.

First, begin by calculating the current excited on the reflector surface due to an incident plane

wave. This current in turn radiates a scattered field, part of which is detected by the feed. The total electric field at the feed is given by

$$\bar{E}^f = -\frac{\pi}{2}\int_{-a}^{a} J_z(\rho')\, H_o^{(2)}\left(2\pi\sqrt{(x_m-x_f)^2+(y_m-y_f)^2}\right) d\rho' \; +$$

$$\delta(\phi_o) e^{j2\pi(x_f\cos\phi_o + y_f\sin\phi_o)} \qquad (2.4\text{-}1)$$

where

$(x_m\ ,\ y_m)$ are the segment midpoints on the parabola

$(x_f\ ,\ y_f)$ are the locations of the feed elements

$\delta(\phi_o,f)$ is the blockage factor $= \begin{cases} 1 & \text{when } 0 \le \phi_o \le \phi_{b1} \text{ and } \phi_{b2} \le \phi_o \le 2\pi \\ 0 & \text{otherwise} \end{cases}$

ϕ_o is the incident field angle

The first term in (2.4-1) is the field scattered by the reflector surface. The second term is the incident field. It is only present when not blocked by the reflector surface. The blockage angles for particular elements in the feed are

$$y>0: \qquad \phi_{b1} = \tan^{-1}\left(\frac{YEND(1) - y_f}{XEND(1) - x_f}\right) \qquad (2.4\text{-}2)$$

$$y<0: \qquad \phi_{b2} = \tan^{-1}\left(\frac{YEND(N+1) - y_f}{XEND(N+1) - x_f}\right) \qquad (2.4\text{-}3)$$

The endpoints of the reflector are given by $\left(XEND(1)\ ,\ YEND(1)\right)$ and $\left(XEND(N+1)\ ,\ YEND(N+1)\right)$. Once $\bar{E}^f$ is found for each element, the sum of the element fields is

$$\bar{E}^T = \sum_{n=1}^{NE} w_n P(\phi)\, \bar{E}_n^f \qquad (2.4\text{-}4)$$

For this report, the normalized element weights, w_n, are found by conjugate matching the field scattered by the reflector at $\phi_o = 0^\circ$. The element patterns $P(\phi)$, are function of ϕ. All the antenna patterns are normalized to the peak of the far field pattern of a strip having the same diameter as the reflector and constant amplitude current.

3. BACKSCATTERING PATTERNS OF CORNER REFLECTORS

To validate the computer software, the computed backscattering pattern of a 90° corner reflector was compared with data from experimental measurements (Figure 3.1). The agreement between the computed and measured plots is quite good. Figure 3.2 is a graph of the computed backscattering pattern of the 90° corner reflector.

Large backscattering returns are expected when an incident angle is normal to one of the flat faces (specular return) of the reflector. These angles are found to be

$$\phi_o = \pm 90^\circ \pm \frac{1}{2}\phi_c \qquad (1)$$

When $\phi_c > 90^\circ$ one side of the reflector never blocks the other side from an incident field that is normal to its face. Thus, the RCS of the reflectors in Figures 3.2 ($\phi_c = 90^\circ$) and 3.3 ($\phi_c = 140^\circ$) are the same at the angles given in (1). As ϕ_c decreases, one side of the reflector blocks the other side from a normally incident wave. Consequently, the large specular return of the partially blocked side decreases as ϕ_c decreases. The specular return for the 80° corner reflector at 50° (Figure 3.4) is not as large as the corresponding specular returns for the corner reflectors with $\phi_c > 90^\circ$. An even larger decrease is noted for the 60° corner reflector (Figure 3.5). The specular return from the backside of the corner reflectors is the same for all values of ϕ_c. The 90° and 60° corner reflectors show a significant return at $\phi_o = 0^\circ$ due to constructive addition of the electromagnetic waves scattering from the sides. The 80° corner reflector has a low return at $\phi_o = 0^\circ$ because the scattered waves do not add constructively .

If the entire 90° corner reflector were made from a resistive sheet having a normalized resistivity of $\eta = 1.0$, then the backscattering RCS would look like the graph in Figure 3.6. This RCS pattern is nearly identical to the one in Figure 3.2 from 40° to 180°, except this pattern is approximately 10dB lower in amplitude. A major difference occurs from 0° to 40°. The resistive

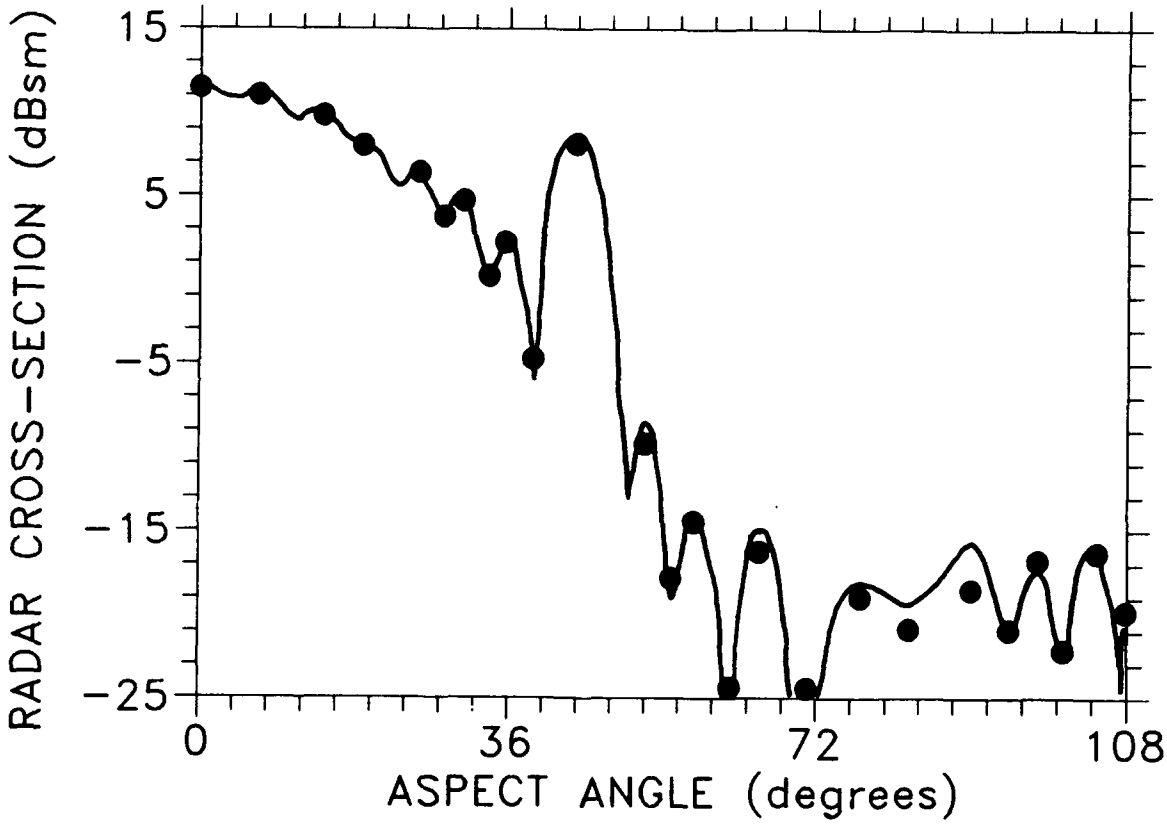

Figure 3.1 Measured backscattering patterns of a corner reflector having 5.6λ square sides and $\phi_c \approx 90$ [6]. The dots on the plot are calculated results from Figure 3.3.

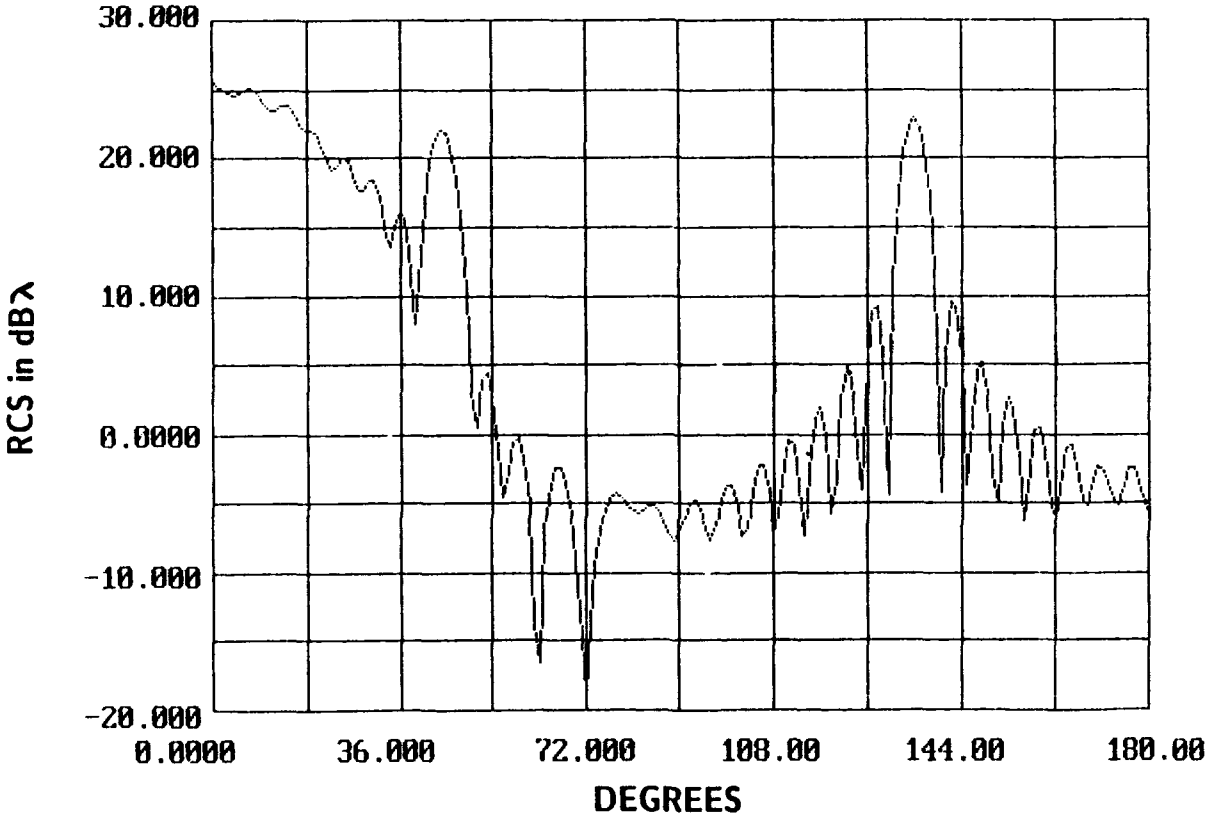

Figure 3.2 Backscattering pattern of a two-dimensional perfectly conducting 90 corner reflector having 5.6λ sides.

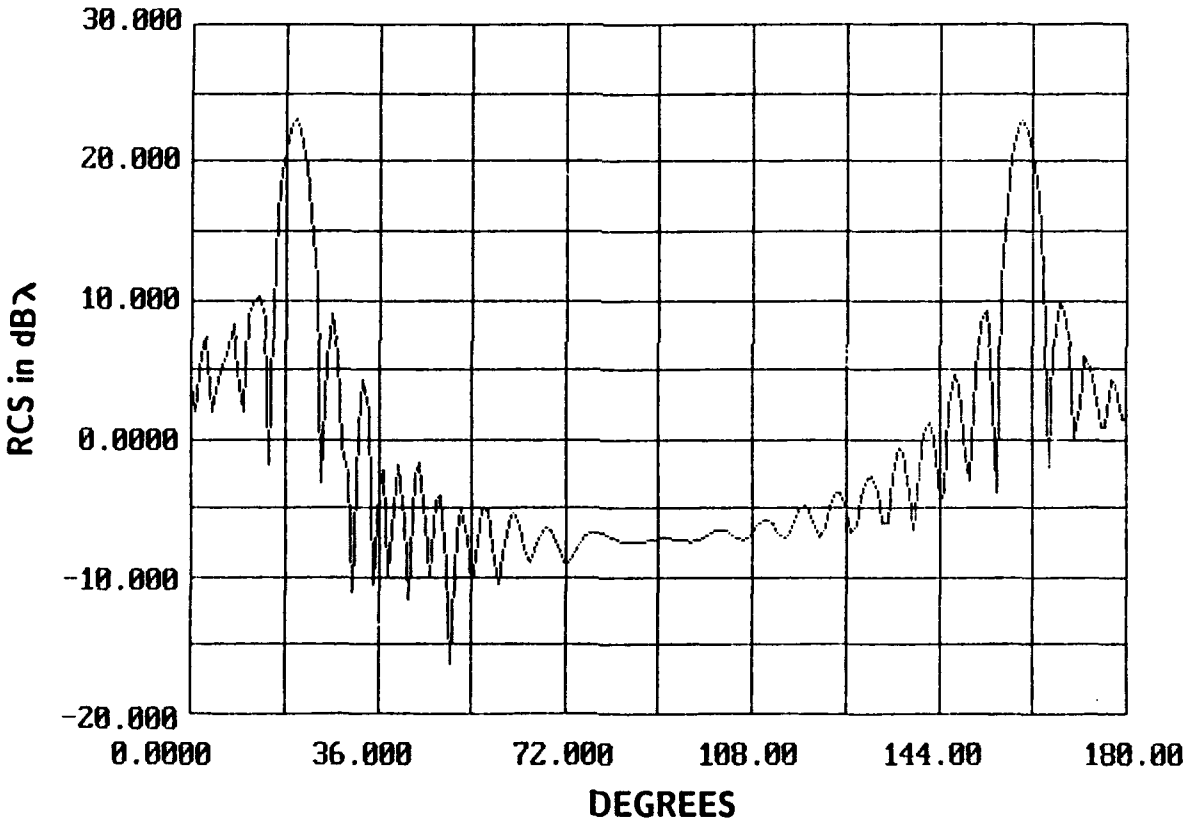

Figure 3.3 Backscattering pattern of a perfectly conducting two-dimensional corner reflector having 5.6λ sides and Φ_c=140°.

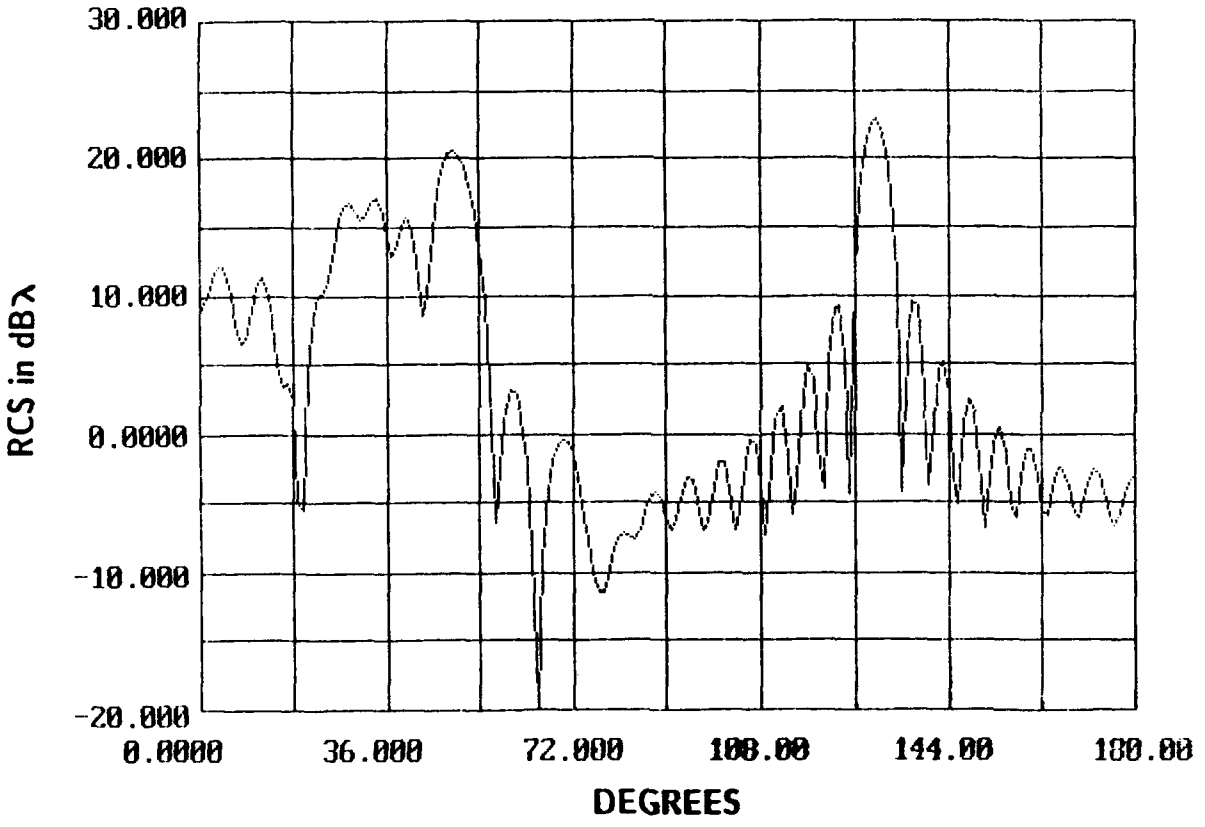

Figure 3.4 Backscattering pattern of a perfectly conducting two-dimensional corner reflector having 5.6λ sides and ϕ_c=80°.

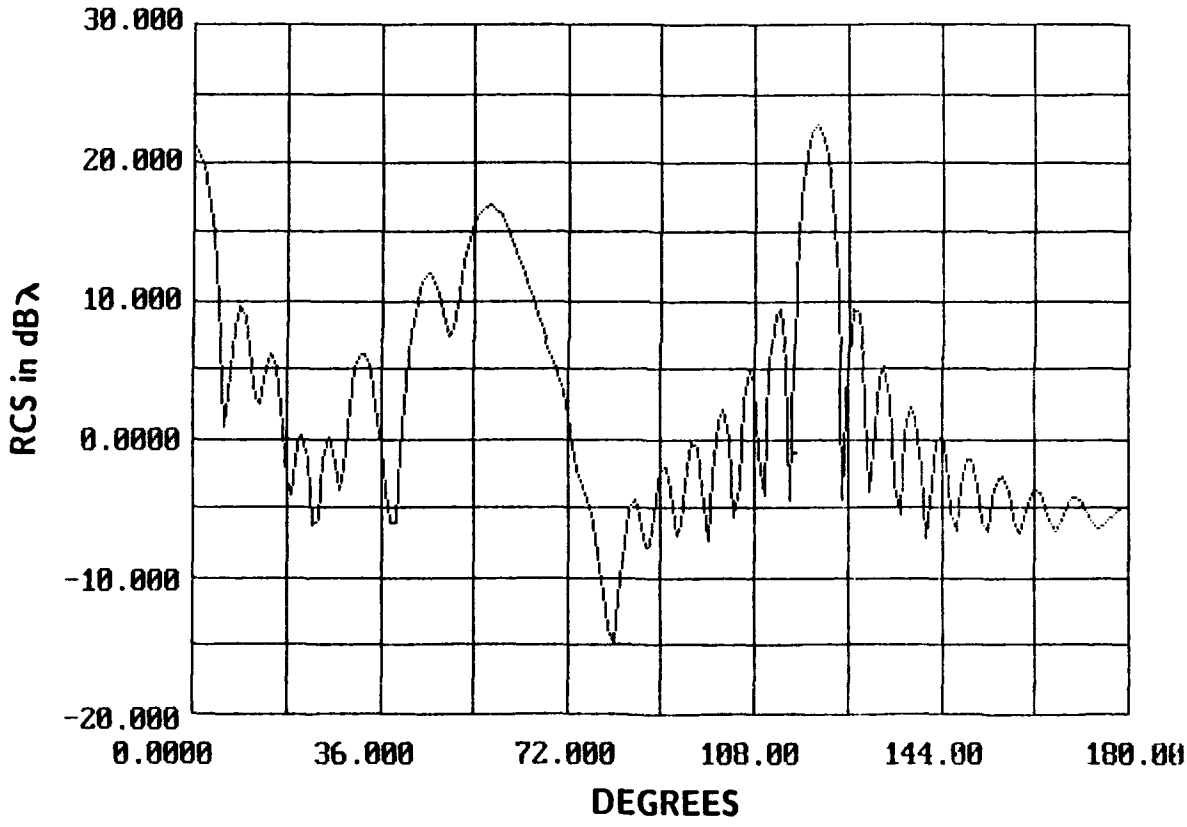

Figure 3.5 Backscattering pattern of a perfectly conducting two-dimensional corner reflector having 5.6λ sides and Φ_c=60°.

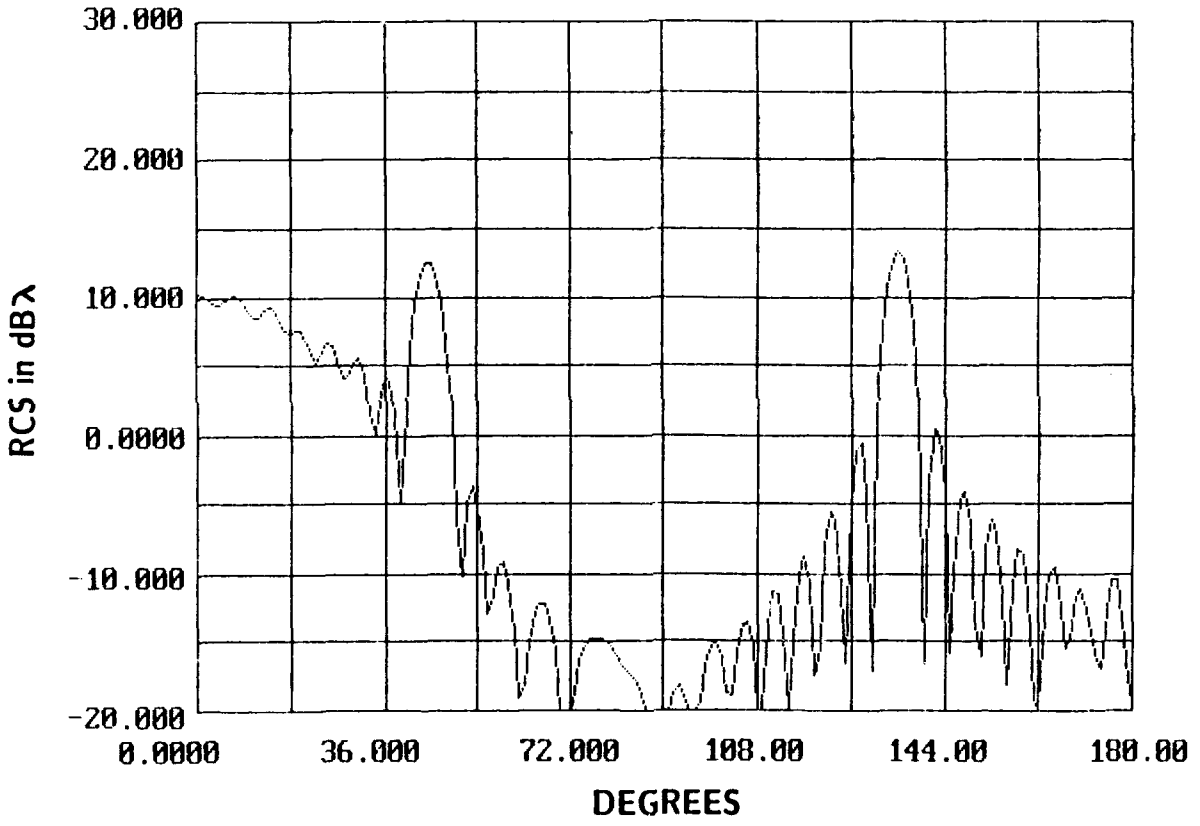

Figure 3.6 Backscattering pattern of a two-dimensional 90 corner reflector having 5.6λ sides and a resistivity of 1.0.

reflector has a lower return at these angles, because the electormagnetic wave has multiple reflections from the lossy sides. Note that the specular returns at 45° and 90° are nearly the same height, but the return at 0° is now lower than the specular returns.

The next two figures (Figure 3.7 and Figure 3.8) show backscattering RCS patterns for 90° corner reflectors with quadratic resistive tapers. These tapers are perfectly conducting at the vertex of the corner and gradually become more resistive toward the edges. An equation for the resistive taper is given by

$$\eta(d) = b\left(\frac{d}{D/2}\right)^2 \qquad (1)$$

where

d = distance along the surface of the corner reflector

D = total length of one side of the corner reflector

b = maximum resistivity at the edge

Figure 3.7 is the backscattering pattern from a 90° corner reflector with a quadratic taper that has an edge resistivity η=0.5 (b=0.5). This resistive taper produces a small decrease in the RCS ($\simeq$0.5 dBλ) at 0° and in the specular directions. The sidelobe region beyond 135° is virtually unchanged from RCS sidelobes in the same region for the perfectly conducting corner reflector. The sidelobes between 45° and 135° are as much as 3 dBλ lower than the same sidelobes of the backscattering pattern of the perfectly conducting corner reflector. Figure 3.8 is the backscattering pattern from a 90° corner reflector with a quadratic taper that has an edge resistivity η=2.0 (b=2.0). Compared to the perfectly conducting backscattering pattern, this pattern shows an approximately 2 dBλ decrease in the major lobes and as much as a 6 dBλ decrease in the sidelobes. There is no noticable change in the sidelobes above 160°.

The RCS of the perfectly conducting corner reflector changes when part of the reflector is made from resistive strips. Consider a 90° corner reflector with sides that are resistive 1λ from each edge.

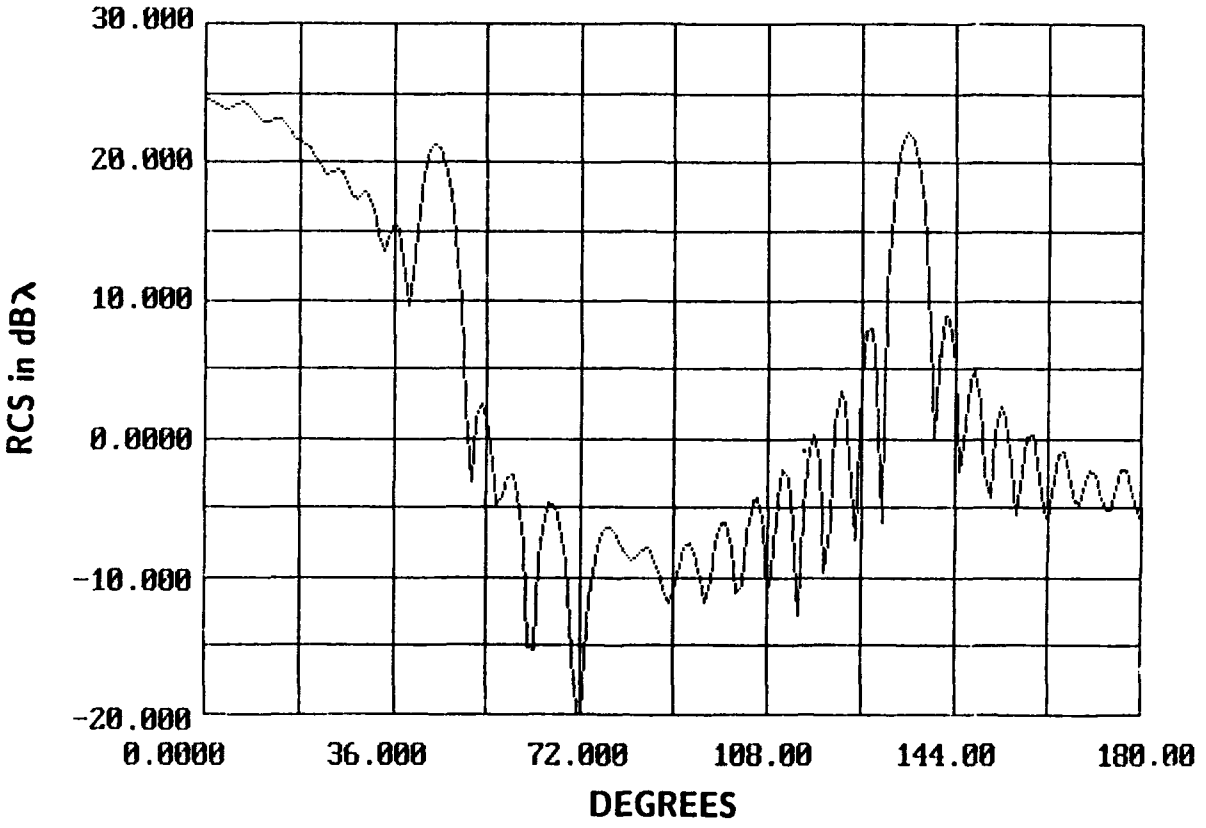

Figure 3.7 Backscattering pattern of a two-dimensional 90° corner reflector having 5.6λ sides and a resistivity of $\eta(d)=0.5d^2$.

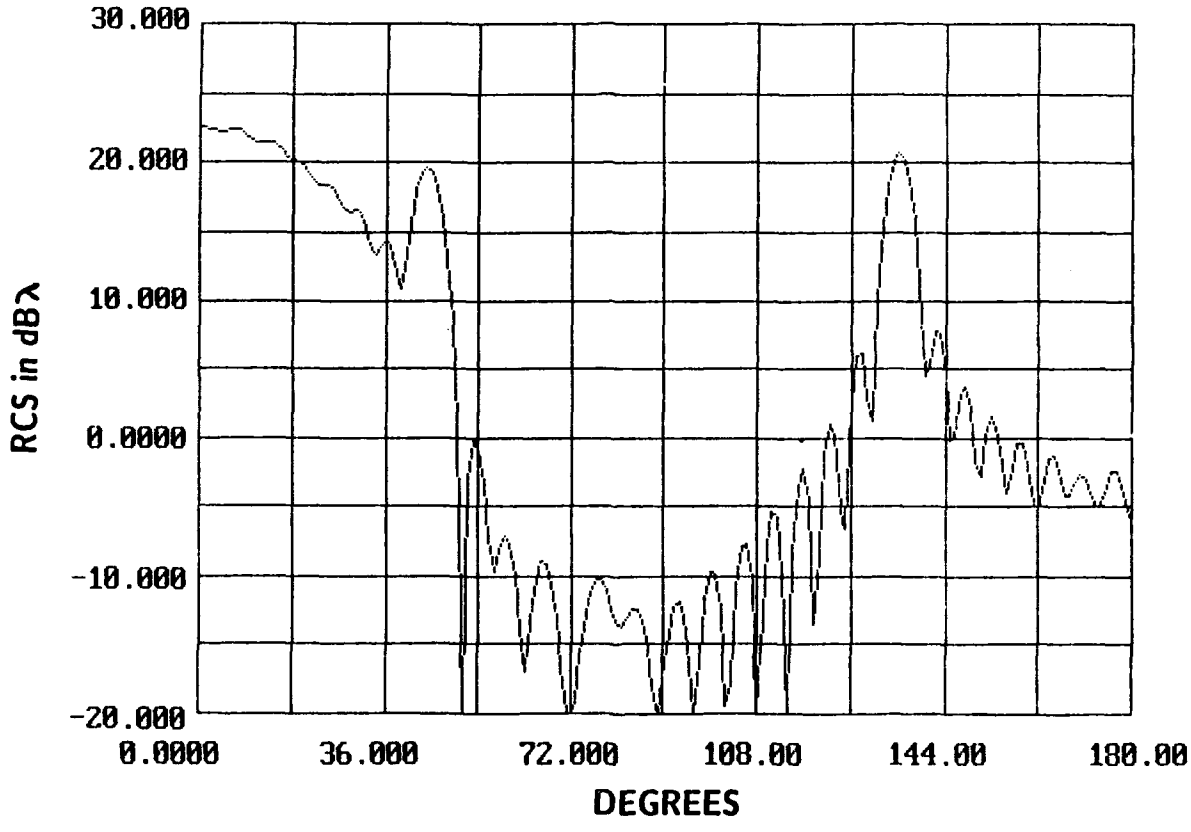

Figure 3.8 Backscattering pattern of a two-dimensional 90°_{2} corner reflector having 5.6λ sides and a resistivity of $\eta(d)=2d^{2}$.

Figure 3.9 shows the backscattering patterns of the edge loaded reflectors when η=0.5 and η=2.0. Edge loads with η=2.0 have reduced RCS main lobes while edge loads with η=0.5 have reduced RCS sidelobes. As η increases, this backscattering pattern approaches the backscattering pattern of a corner reflector with sides that are 4.6λ long. Both patterns show an overall decrease in the RCS compared to the perfectly conducting reflector, especially in the 50° to 130°sidelobe region.

The next figure (Figure 3.10) shows the backscattering pattern of a 90° with 5.6λ sides and an edge load with η=1.0. Increasing the size of the edge load while keeping the sides of the reflector 5.6λ long, decreases the RCS of the main lobes. Again, these patterns show an overall decrease in the RCS compared to the perfectly conducting reflector, especially in the 50° to 130° sidelobe region.

The discontinuity between the perfectly conducting reflector and the constant resistive loads produces a discontinuity in the current density. This current density discontinuity prevents the backscattering pattern from having very low sidelobes. The resistivity discontinuity is eliminated by smoothly tapering the resistivity from perfectly conducting to highly resistive at the edges. Such a resistive taper produces a corresponding current density taper.

Figure 3.11 shows the backscattering patterns of the corner reflector as the resistivity is tapered from perfectly conducting at 1.0λ from the edges to values of η= 0.5, 1.0, and 2.0 at the edges. Increasing the resistivity at the edges does not noticeably change the backscattering main lobes but does lower the sidelobes. Extending the taper from 1.0λ from the edges to 2.0λ from the edges while keeping the maximum value of η the same produces little change to the backscattering pattern (Figure 3.12).

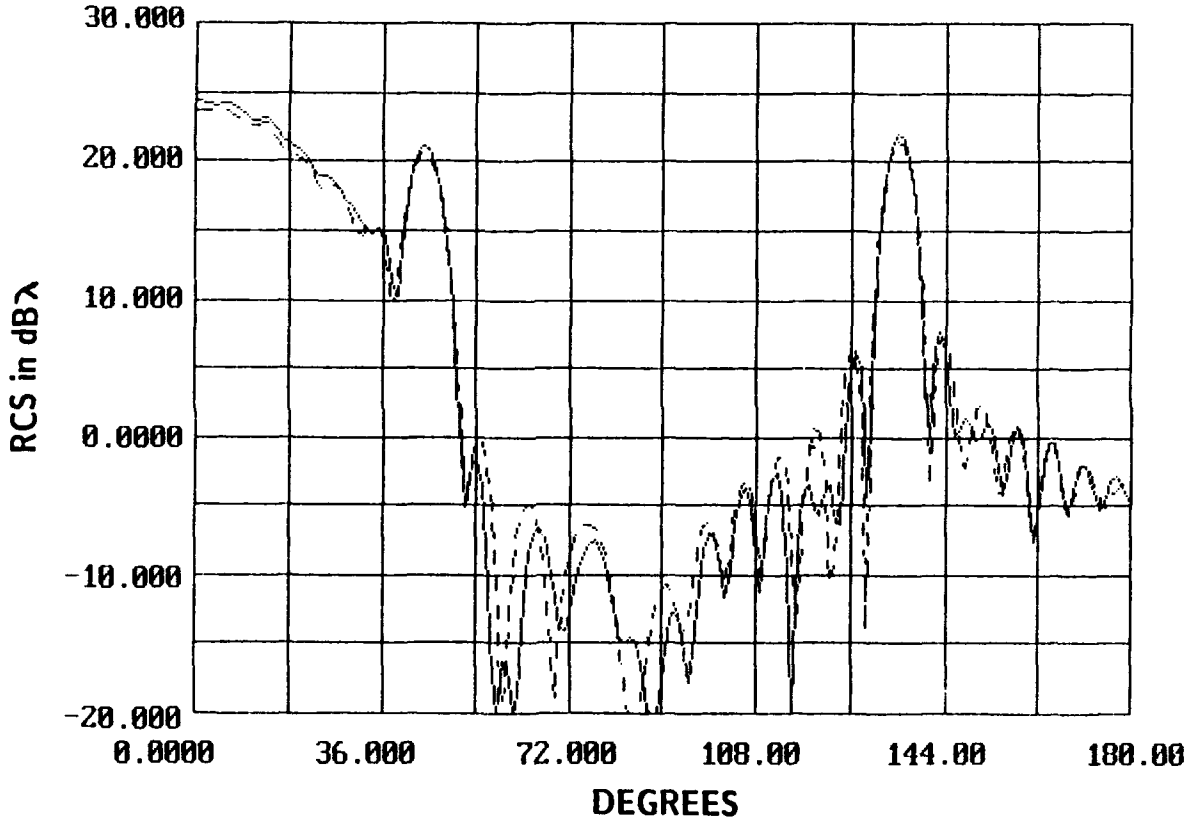

Figure 3.9 Backscattering patterns of two-dimensional 90 corner reflectors having 5.6λ sides and a constant resistive load 1λ from the edges — η=0.5 and --- η=2.0.

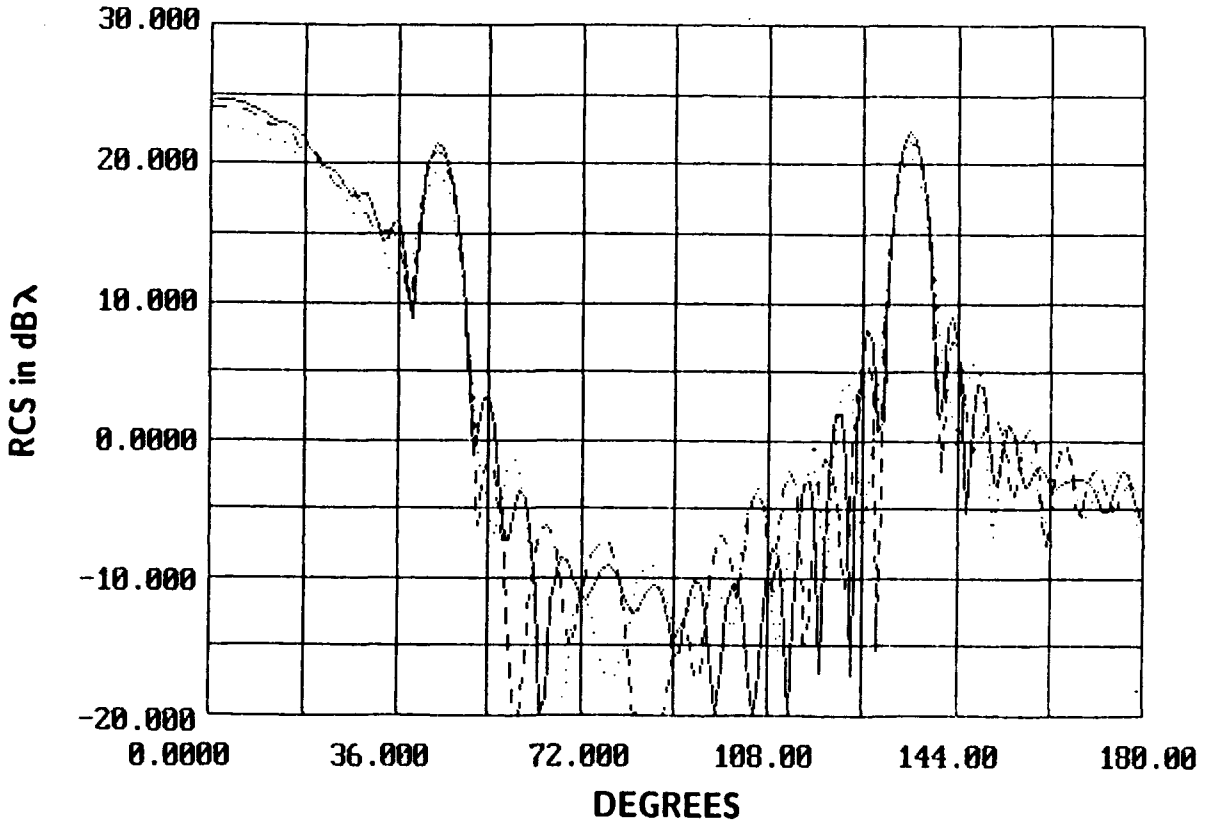

Figure 3.10 Backscattering patterns of two-dimensional 90° corner reflectors having 5.6λ sides and a constant resistive load η=1.0. — 0.5λ from the edge, --- 1.0λ from the edge, ··· 2.0λ from the edge.

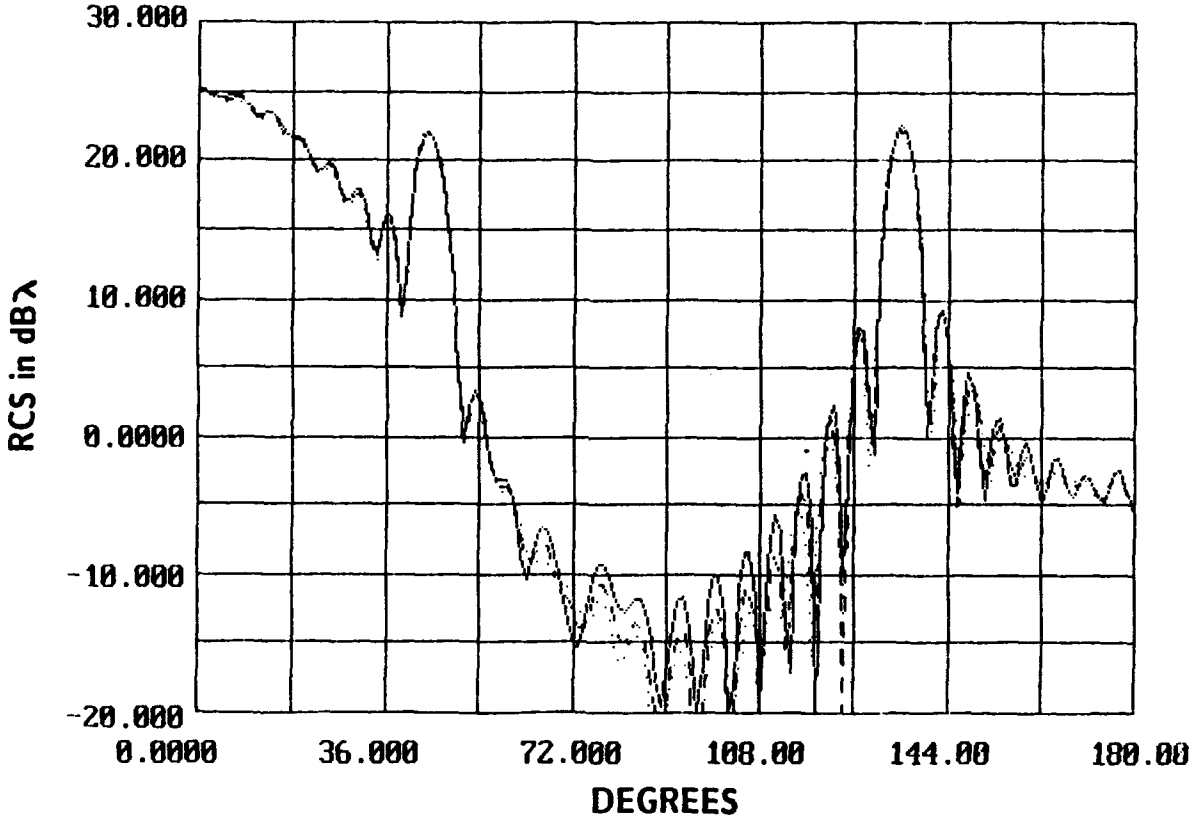

Figure 3.11 Backscattering patterns of two-dimensional 90° corner reflectors having 5.6λ sides and a quadratic resistive taper 1.0λ from the edges. — η_{max}=0.5, ---η_{max}=1.0, ···η_{max}=2.0.

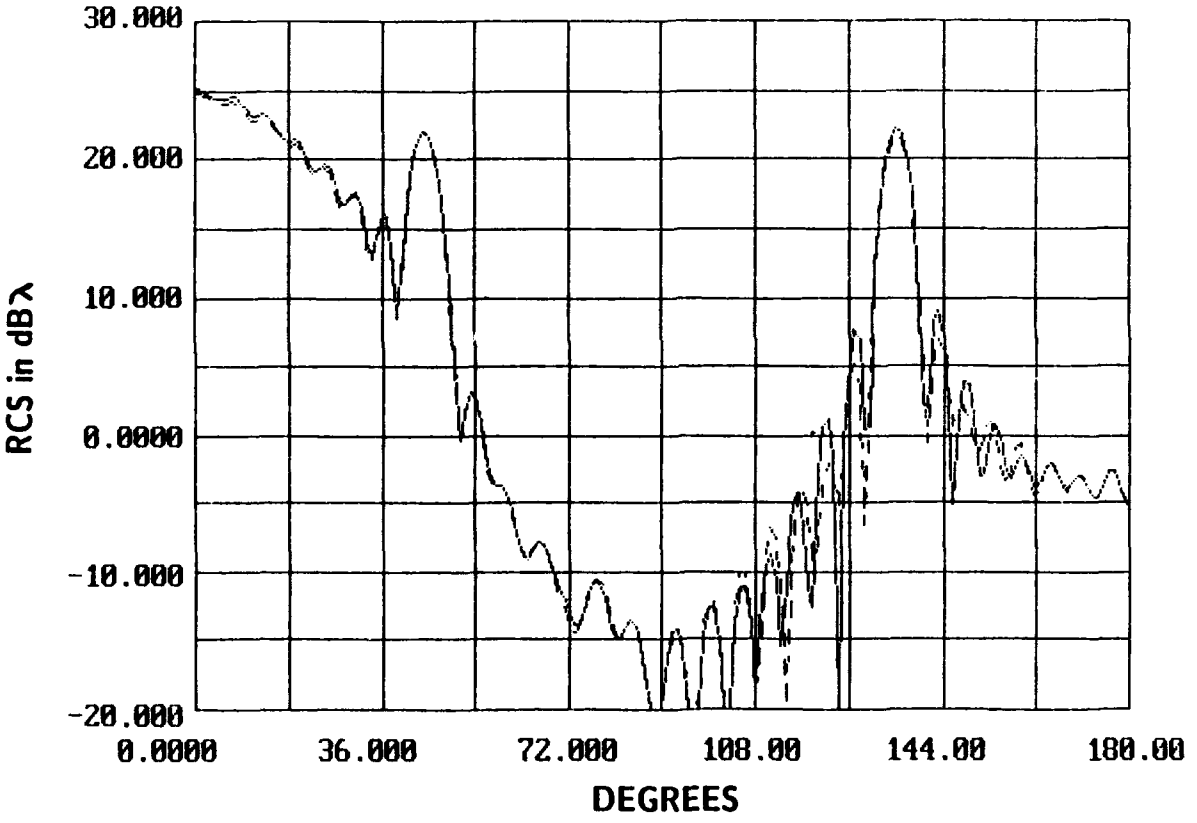

Figure 3.12 Backscattering patterns of two-dimensional 90° corner reflectors having 3.6λ sides and a quadratic resistive taper at the edges with η_{max}=1.0. — 1.0λ from the edge, ---2.0λ from the edge.

4. BACKSCATTERING PATTERNS OF PARABOLIC REFLECTORS

This chapter presents some calculated backscattering patterns from two-dimensional parabolic reflector antennas. No experimental data was found in the literature to validate these theoretical patterns.

The backscattering pattern of a two-dimensional perfectly conducting parabolic surface having an aperture length of 10λ and a focal length of 5λ is shown in Figure 4.1. This pattern shows rather large returns for backscattering angles close to the x-axis. The RCS pattern varies rapidly from 0° to 90°, while the RCS pattern is very smooth from 90° to 180°.

If the entire parabola were made from a resistive sheet having a normalized resistivity of η=1.0, then the backscattering RCS would look like the graph in Figure 4.2. This RCS pattern is nearly identical to the one in Figure 4.1, except this pattern is approximately 10dB lower in amplitude. The one exception occurs near a 90° angle of incidence. Here, the RCS is an additional 5 dB less than the RCS of the perfectly conducting parabola. Another difference is the RCS pattern for the resistive parabola is not as smooth as the RCS pattern of the perfectly conducting parabola for incident angles between 90° and 180°.

Figure 4.3 is the backscattering pattern from a parabola with a quadratic taper that has an edge resistivity η=0.5 (b=0.5). This resistive taper did not lower the returns at 0° and 180° but did lower the returns by 3 to 10 dB between 18° and 162°. Figure 4.4 is the backscattering pattern of a parabola with a quadratic taper that has a resistivity of η=2.0 (b=2) at the edge. This taper lowered the return at 0° and 180° by about 2 dB, while elsewhere it substantially lowered the sidelobes.

Backscattering from the parabola may also be reduced by placing resistive loads on the edges. Figure 4.5 compares the backscattering patterns of reflectors with the resistive loads for the last 1λ of the surface. The loads do not substantially alter the patterns. The η=0.5 load has slightly higher backscattering main lobes and lower backscattering sidelobes than the η=2.0 load. Figure 4.6 displays

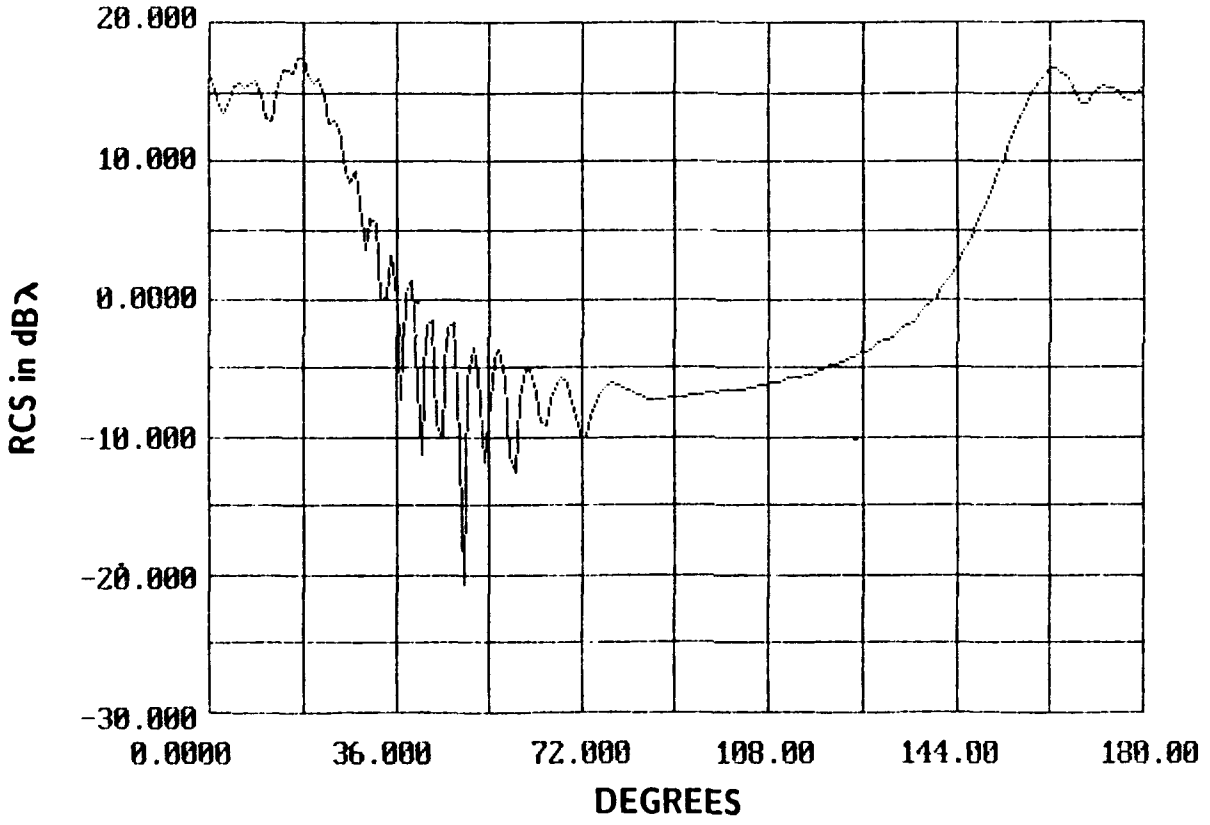

Figure 4.1 Backscattering pattern of a two-dimensional perfectly conducting parabolic reflector having a diameter of 10λ and a focal length of 5λ.

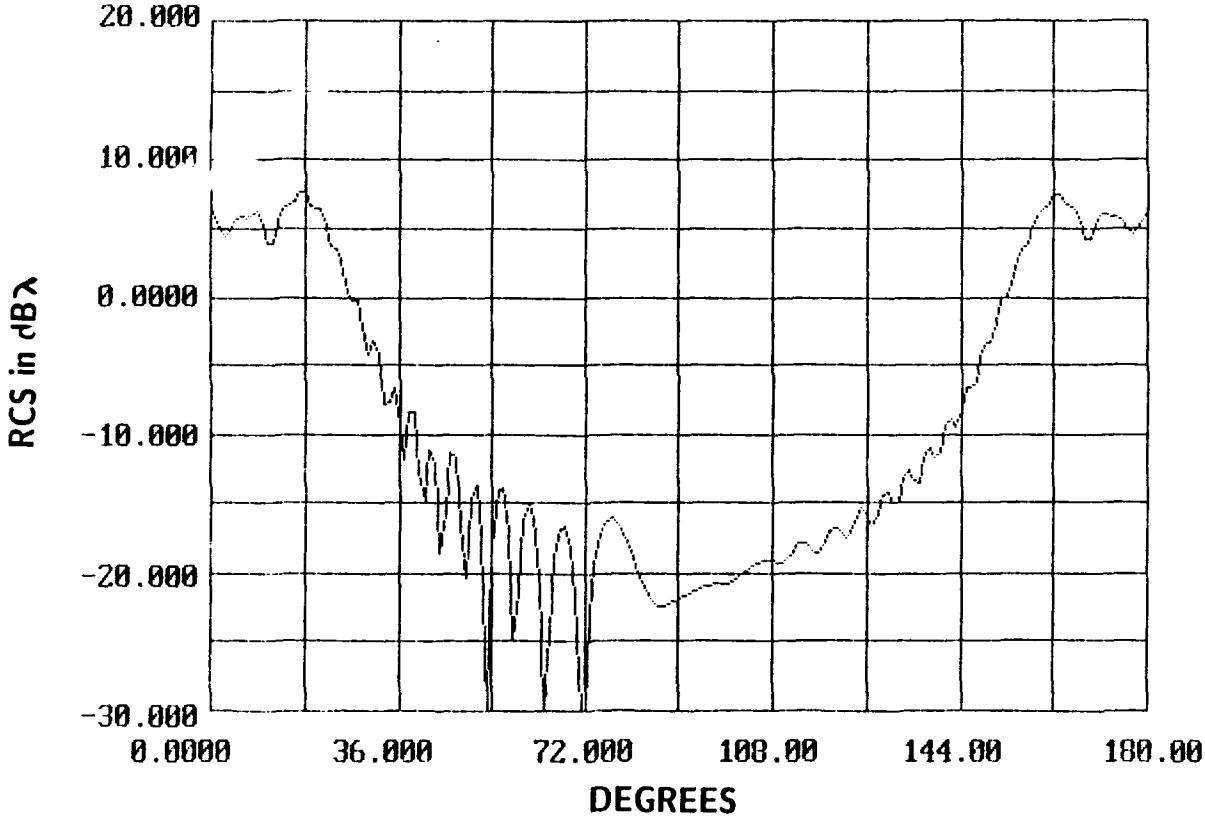

Figure 1.2 Backscattering pattern of a two-dimensional reflector having a diameter of 10λ and a focal length of 5λ and a resistivity of 1.0.

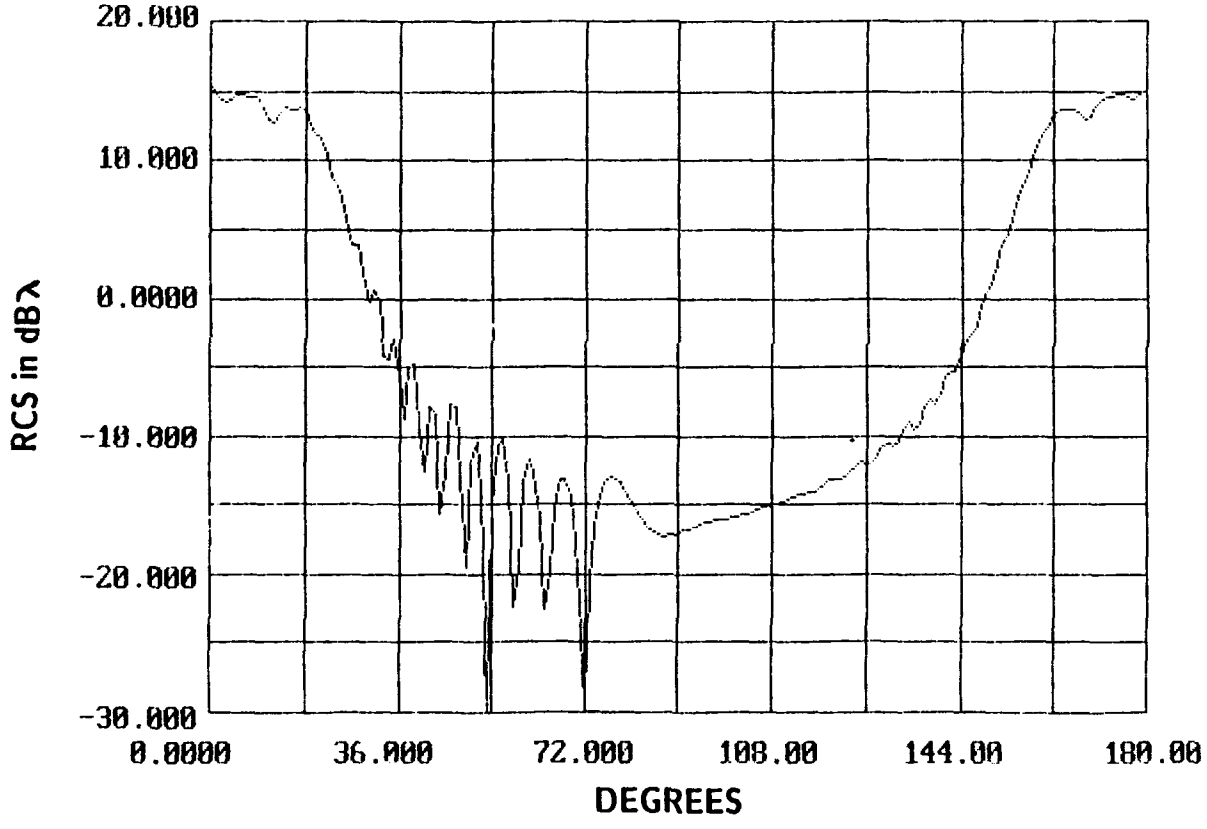

Figure 4.3 Backscattering pattern of a two-dimensional parabolic reflector having a diameter of 10λ and a focal length of 5λ and a quadratic resistive taper that starts with η=0.0 at the vertex and cases until η=0.5 at the edges.

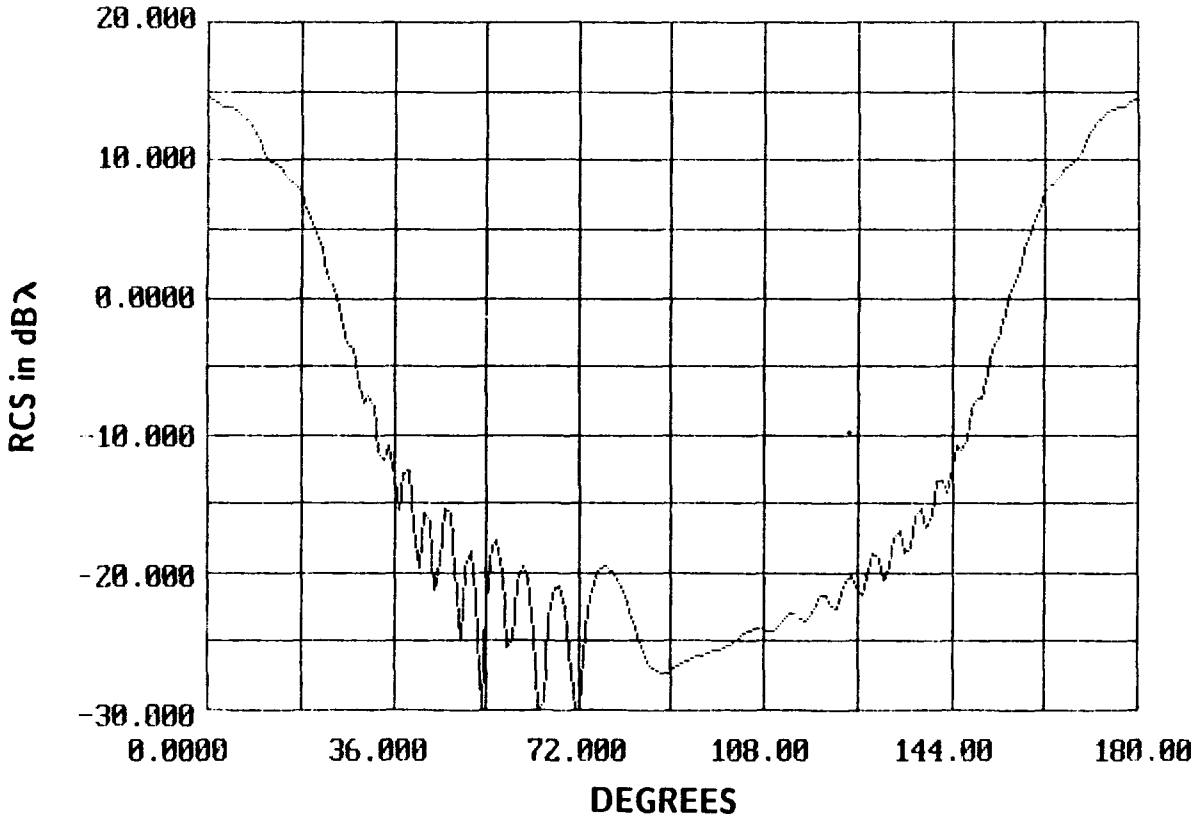

Figure 4.1 Backscattering pattern of a two-dimensional parabolic reflector having a diameter of 10λ and a focal length of 5λ and a quadratic resistive taper that starts with η=0.0 at the vertex and increases until η=2.0 at the edges.

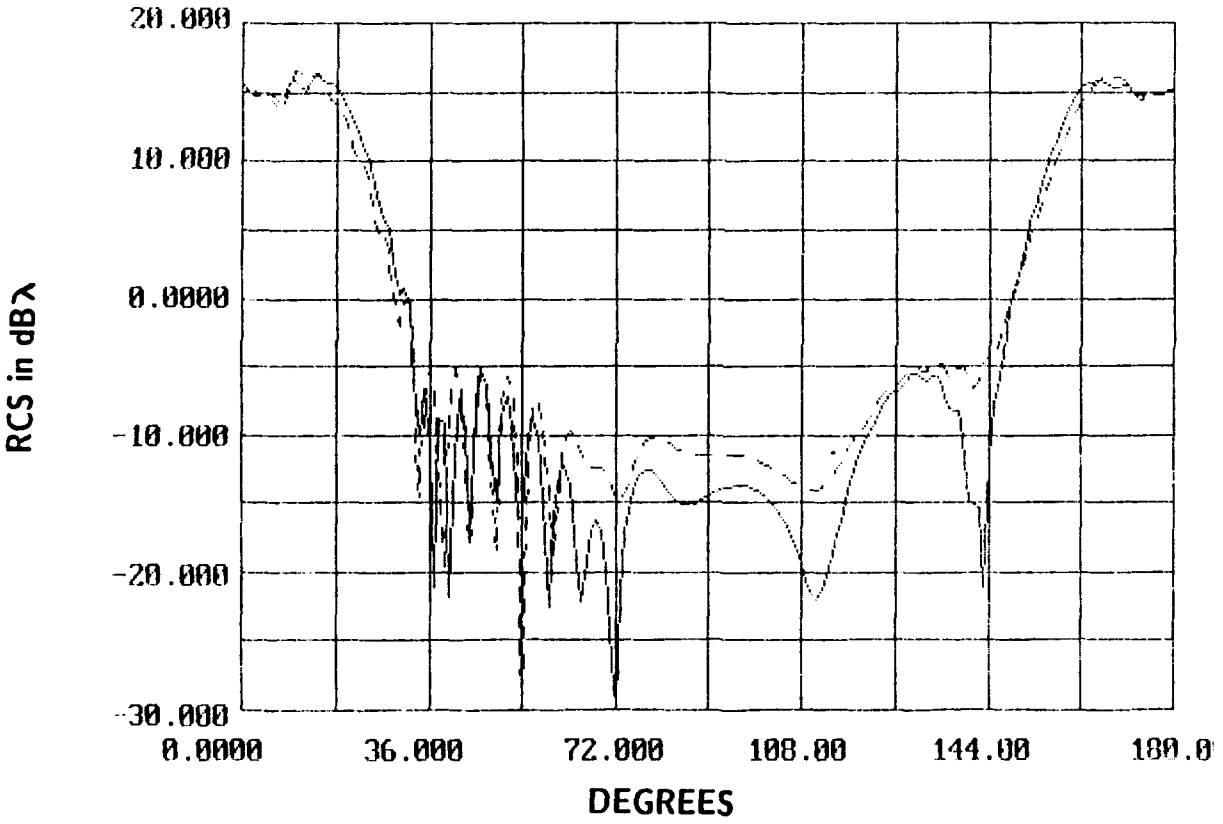

Figure 4.5 Backscattering patterns of a two-dimensional parabolic reflector having a diameter of 10λ and a focal length of 5λ and a constant resistive load 1λ from the edges. — η=0.5 and --- n=2.0.

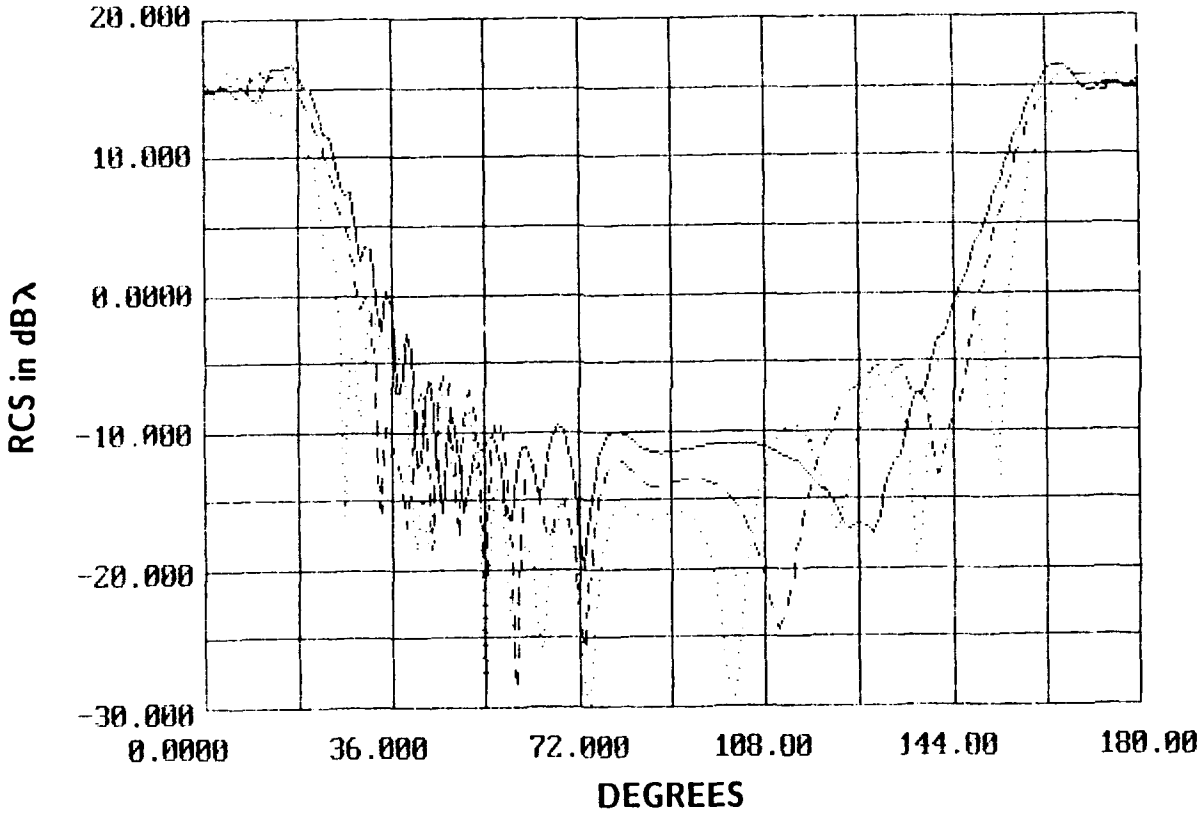

Figure 4.6 Backscattering patterns of a two-dimensional parabolic reflector having a diameter of 10λ and a focal length of 5λ and a constant resistive load η=1.0. —— 0.5λ from the edge, --- 1.0λ from the edge, ···2.0λ from the edge.

the backscattering patterns of parabolas with resistive loads of η=1.0 a distance of 0.5λ, 1.0λ, and 2.0λ away from the edges. As the edge load gets wider, the backscattering main lobes get skinnier and more sidelobes appear. Observe that the response near 0° and 180° has not significantly changed. Compared to the 0.5λ load, the 1.0λ and 2.0λ loads produce at least a 10 dB increase in the scattering patterns near 130°.

Tapering the edge loads shows little change in the main lobe scattering patterns in the 0° to 40° range or in the 172° to 180° range compared to the perfectly conducting reflector (Figure 4.7). Outside these regions, however, a substantial reduction occurs. A heavy taper produces lower sidelobes than a light taper. Extending the width of the taper from 1λ to 2λ while keeping η the same at the edges (b=1) produces little change in the backscattering patterns (Figure 4.8).

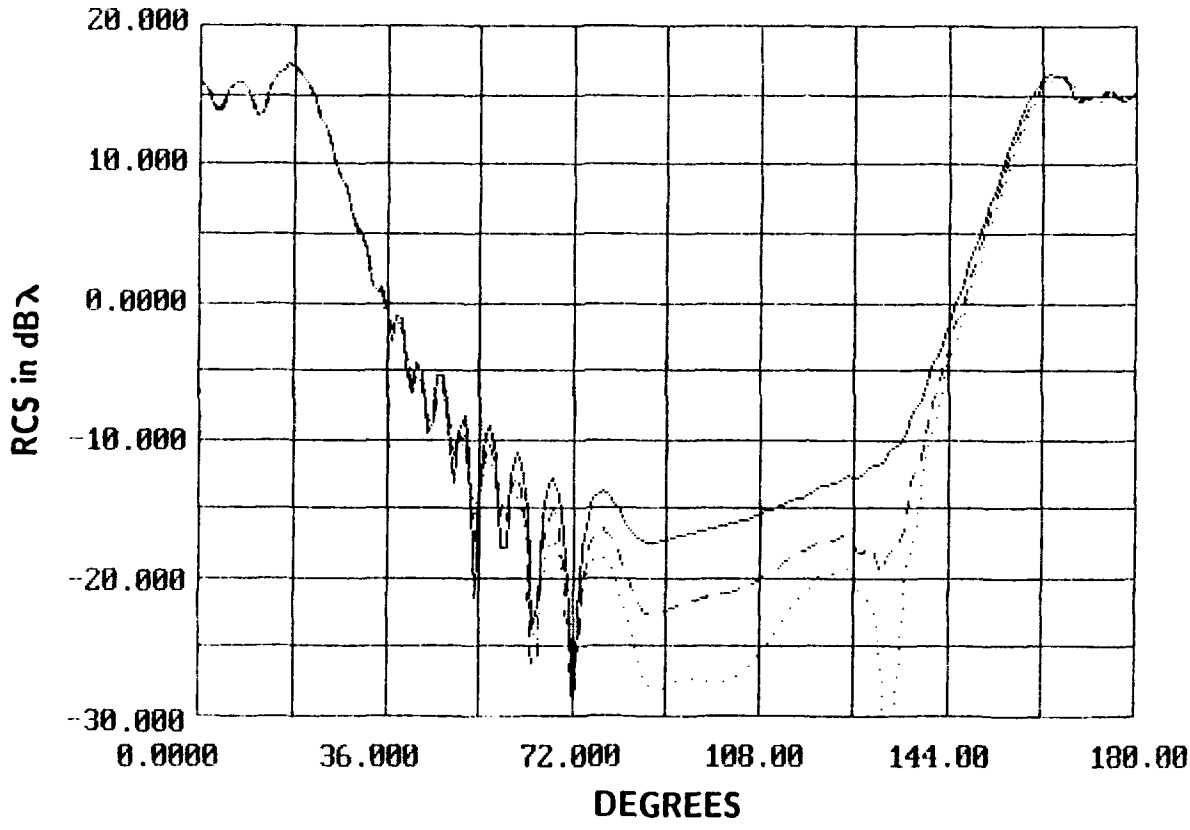

Figure 4.7 Backscattering patterns of a two-dimensional parabolic reflector having a diameter of 10λ and a focal length of 5λ and a quadratic resistive taper 1.0λ from the edges. — η_{max}= 0.5, --- η_{max}=1.0, ···η_{max}=2.0.

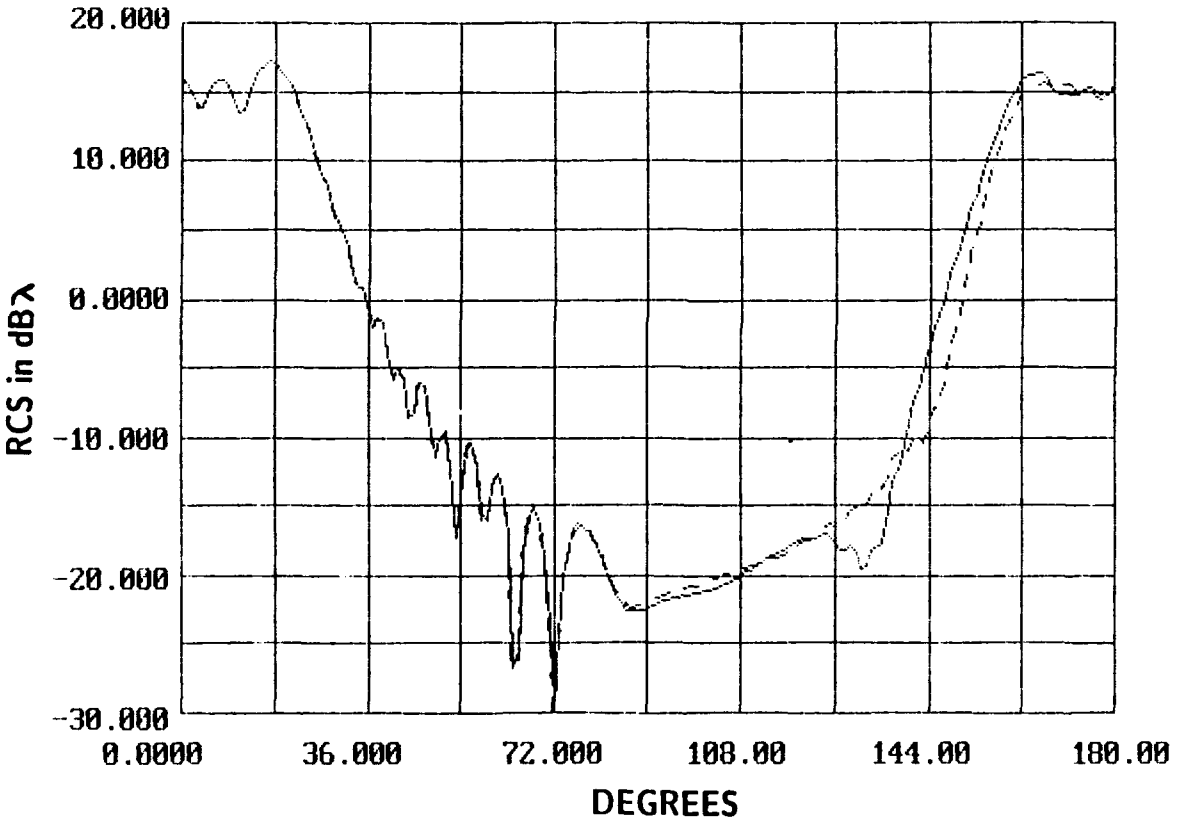

Figure 4.8 Backscattering patterns of a two-dimensional parabolic reflector having a diameter of 10λ and a focal length of 5λ and a quadratic resistive taper at the edges with —— η_{max}= 0.5, ---η_{max}=1.0. — 1.0λ from the edge, ---2.0λ from the edge.

5. ANTENNA PATTERNS OF PARABOLIC REFLECTORS

The calculation of the antenna pattern of a reflector is very similar to the calculation of the scattering pattern. Scattering patterns have the source point and observation point in the far field of the antenna, while antenna patterns have the source point in the far field and the observation point in the near field. Reflector antennas have the interesting property that the Fourier transform of the aperture distribution is the far field, and this far field appears not only very far away from the antenna, but at the focal point as well. The Fourier transform relationship is only approximate at the focal point of the reflector, though. Scattering from the edges of the reflector destroy an exact correspondence. Also, the feed antenna may be a distributed source such as an array or an apperture and not a point source. The Fourier transform relationship holds just at the focal point. Thus, the center element of the array will receive an exact Fourier transform of the aperture distribution, but the other elements will receive an approximation to the Fourier transform. This approximation gets worse the farther away the element is from the focal point.

The equation for a parabolic reflector surface is

$$y^2 = 4fx \tag{1}$$

where f is the focal length of the reflector. A reflector antenna is often specified by the ratio of its focal length to its diameter or its $\frac{f}{D}$ ratio. Typically, the $\frac{f}{D}$ is between .5 and 1.0. This range keeps the feed close to the reflector so it is easy to support, but not so close that feed sidelobes illuminate the reflector surface.

The reflector used as an example in this report has a diameter of 10λ and a focal length of 5λ ($\frac{f}{D}$=0.5). The feed has an electric field pattern given by

$$E(\phi) = \begin{cases} \cos^2\phi & 90^\circ \leq \phi \leq 270^\circ \\ 0 & \text{elsewhere} \end{cases} \tag{1}$$

Figure 5.1 is the antenna pattern for a perfectly conducting reflector surface. Its first sidelobe is 22 dB below its main beam peak. A rather large sidelobe occurs at 114°, because the feed radiation spills over the reflector edge at that point. The peak of this main beam serves to normalize all the far field patterns presented in this section.

The antenna patterns of the reflector were evaluated for the same resistive loads as the scattering patterns were evaluated. Consider the case where the entire reflector is a resistive sheet with η=1.0. The antenna pattern (Figure 5.2) is about 10 dB lower than the perfectly conducting reflector pattern from 0° to 100°. It is 9.4 dB lower at the peak of the main beam. Beyond 100° the pattern is dominated by energy transmitted through the reflector. Sidelobes are lower in this case, but not relative to the peak of the main beam.

Tapering the resistivity of the parabolic reflector produces a substantial reduction to the sidelobe level of the antenna. Figure 5.3 has a quadratic taper with a maximum value of η=0.5 at the edges, and Figure 5.4 has a quadratic taper with a maximum value of η=2.0 at the edges. On the one hand, the higher values of resistive taper produce lower sidelobes (compare Figures 5.3 and 5.4 at angles between 20° and 100°). On the other hand, a larger amount of energy is transmitted through the reflector (compare Figures 5.3 and 5.4 at 140°). The advantage of the lower sidelobes is offset by a reduction in gain of the antenna. The peaks of the main beams in Figures 5.3 and 5.4 are 1.6 dB and 4.2 dB lower than the peak of the main beam in Figure 5.1. This tradeoff is expected though and is acceptable if the sidelobe interference warrants it.

Antenna sidelobes may be lowered without significantly affecting the gain of the antennas by placing a resistive taper on the edges. Figure 5.5 compares the antenna patterns of reflectors having resistive loads for the last 1λ of their length. As the resistivity of the load increases, the sidelobes also increase. This result makes sense because the higher the resistivity, the greater the discontinuity between the perfectly conducting region and the resistive load, hence, the reflector appears to have a smaller diameter. Figure 5.6 displays the antenna patterns of parabolas with resistive loads of η=1.0

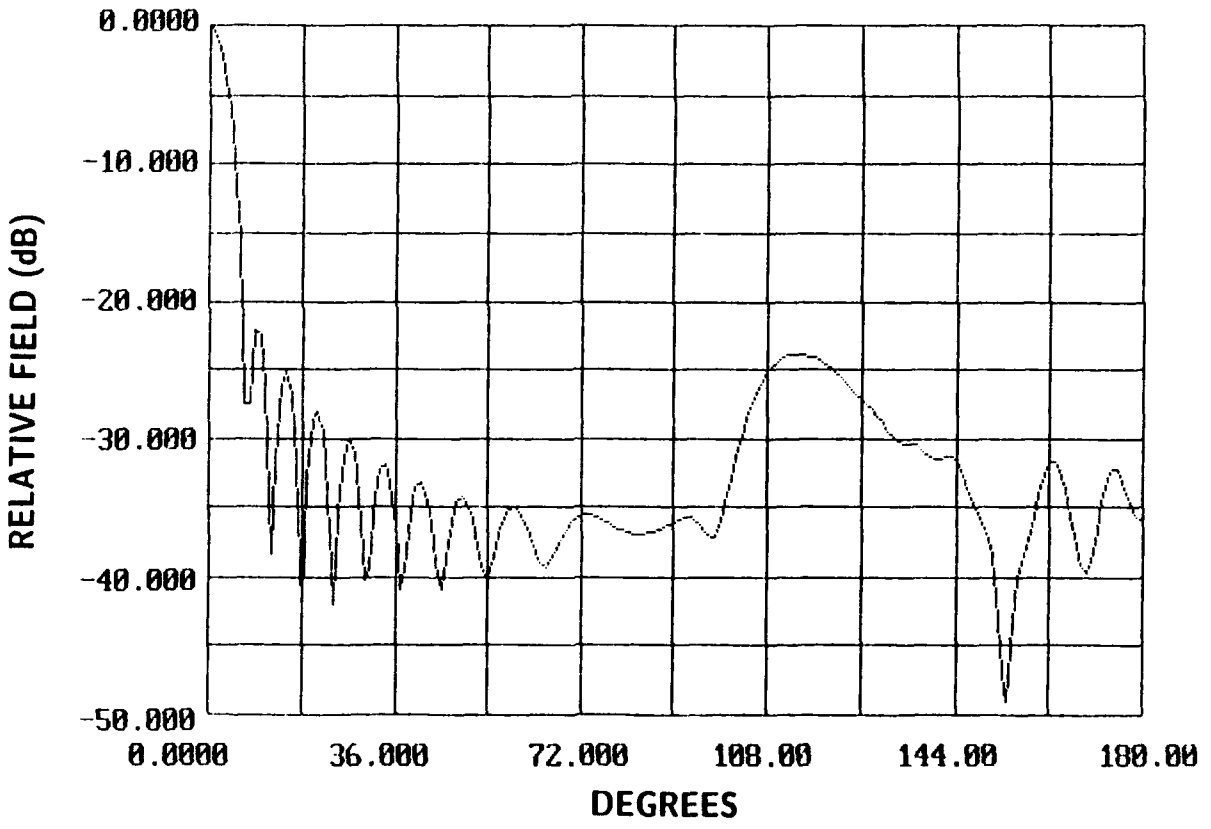

Figure 5.1 Antenna pattern of a two-dimensional perfectly conducting parabolic reflector having a diameter of 10λ and a focal length of 5λ. The feed pattern is given by (5-1).

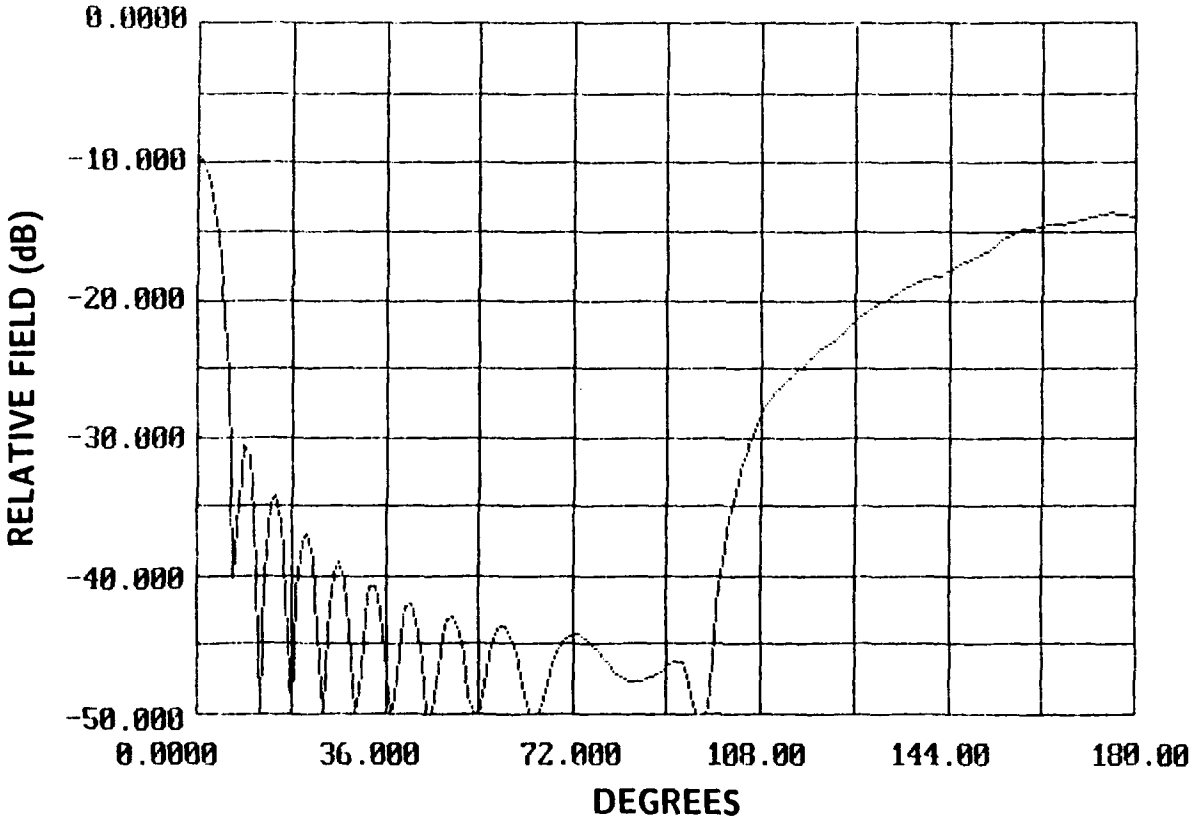

Figure 5.2 Antenna pattern of a two-dimensional reflector having a diameter of 10λ and a focal length of 5λ and a resistivity of 1.0. The feed pattern is given by (5-1).

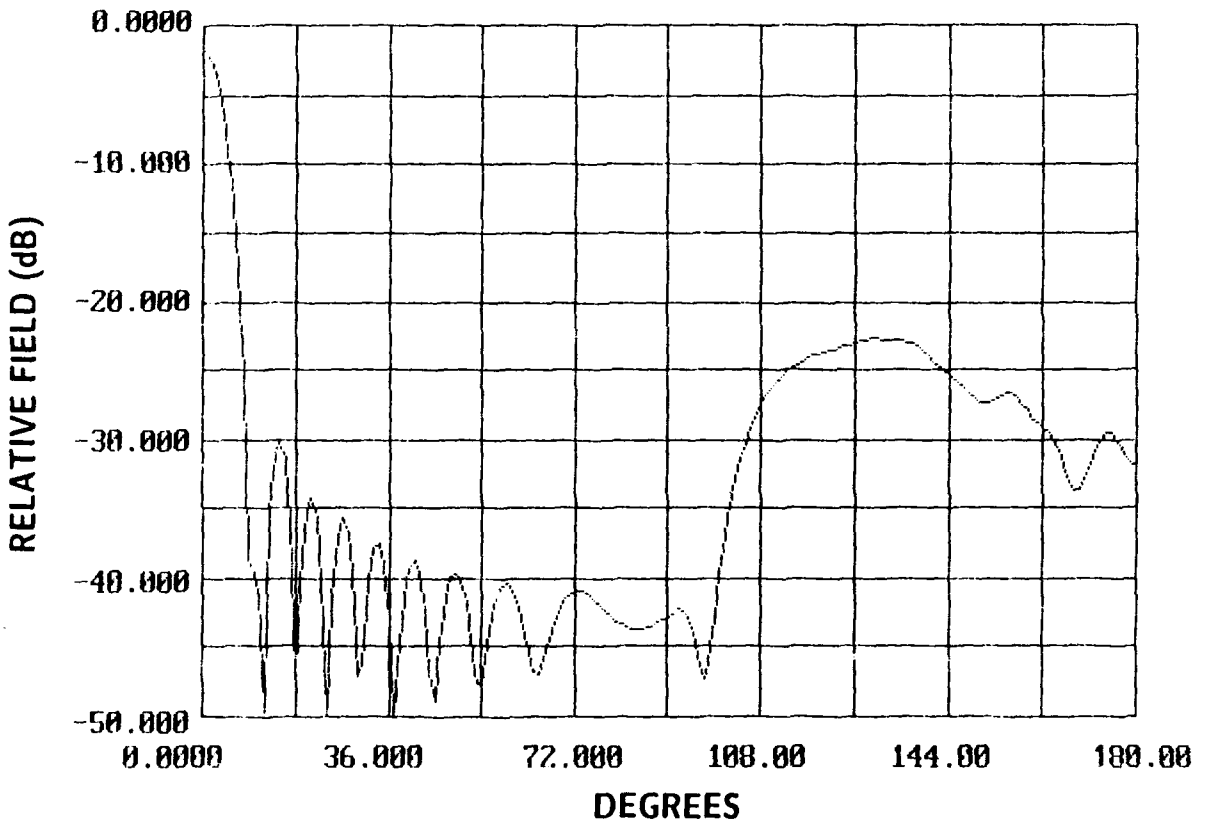

Figure 5.3 Antenna pattern of a two-dimensional parabolic reflector having a diameter of 10λ and a focal length of 5λ and a quadratic resistive taper that starts with η=0.0 at the vertex and increases until η=0.5 at the edges. The feed pattern is given by (5-1).

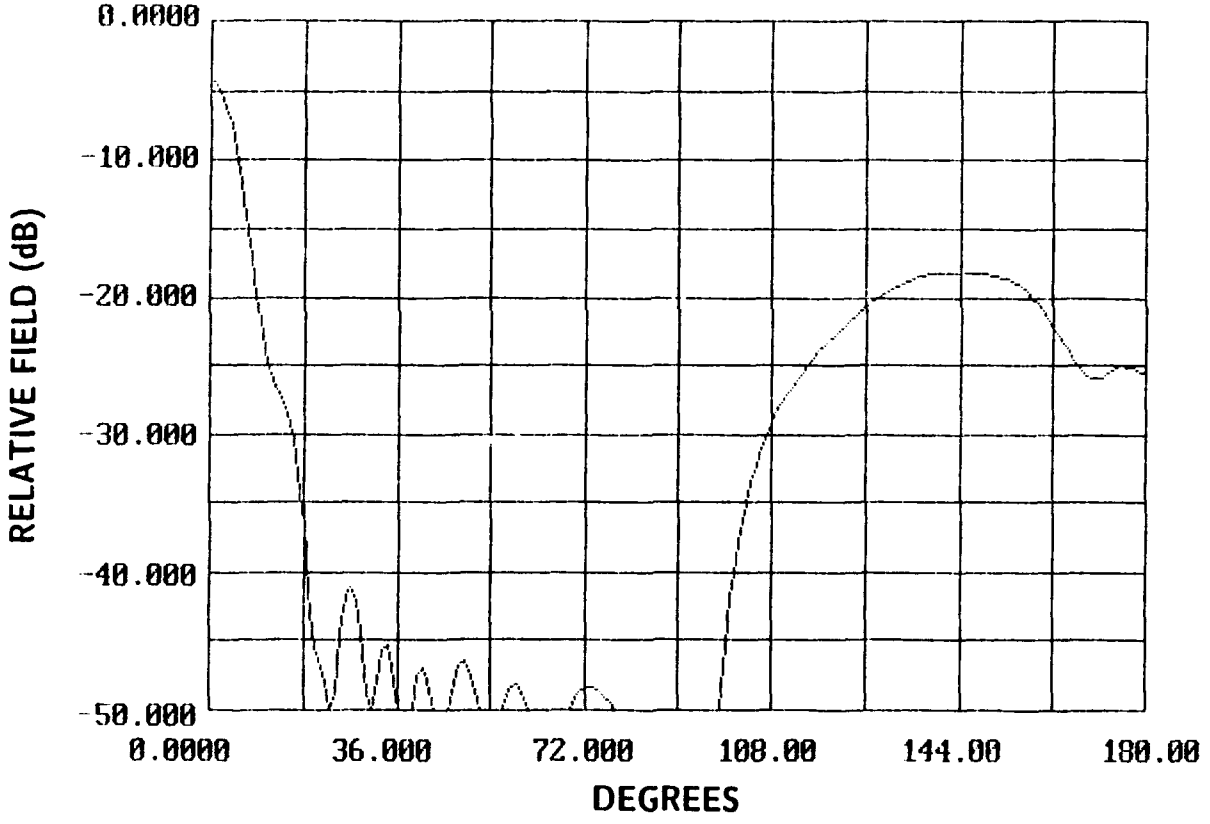

Figure 5.4 Antenna pattern of a two-dimensional parabolic reflector having a diameter of 10λ and a focal length of 5λ and a quadratic resistive taper that starts with $\eta=0.0$ at the vertex and increases until $\eta=2.0$ at the edges. The feed pattern is given by (5-1).

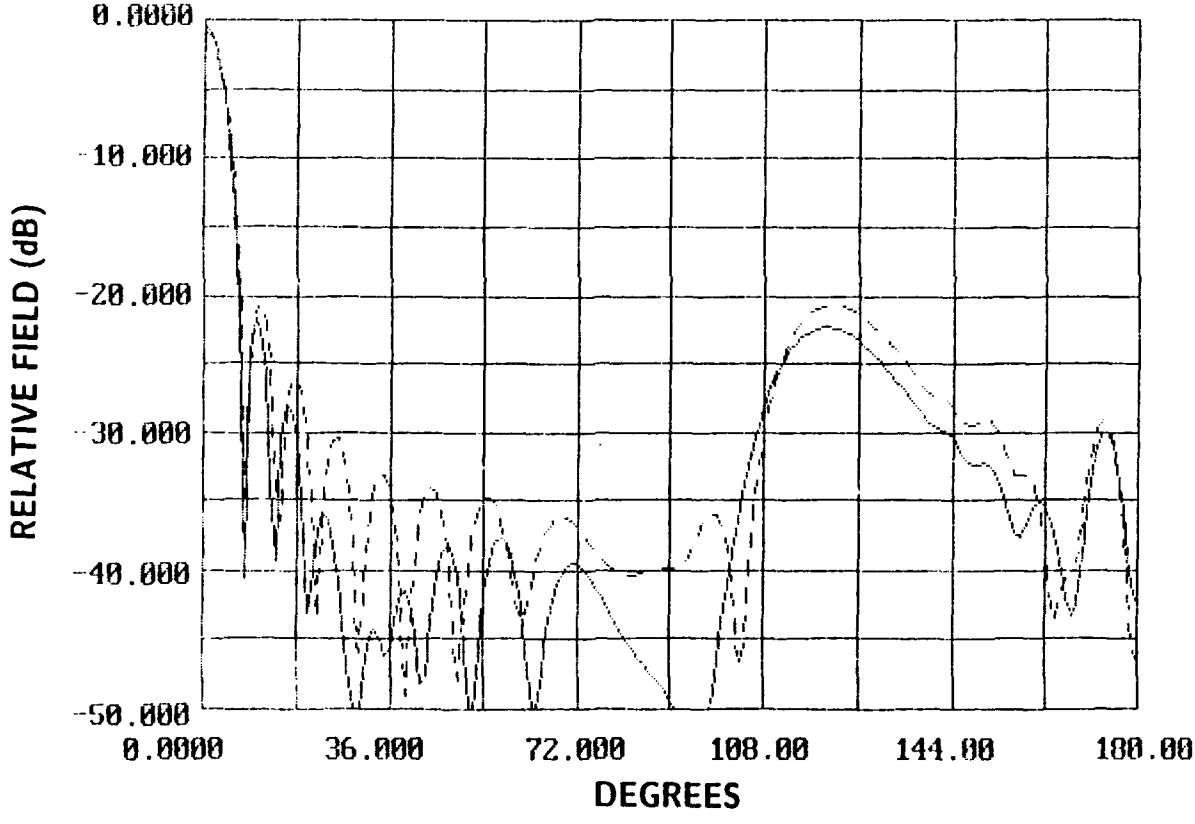

Figure 5.5 Antenna patterns of a two-dimensional parabolic reflectors having a diameter of 10λ and a focal length of 5λ and a constant resistive load 1λ from the edges. The feed pattern is given by (5-1). — η=0.5 and --- η=2.0.

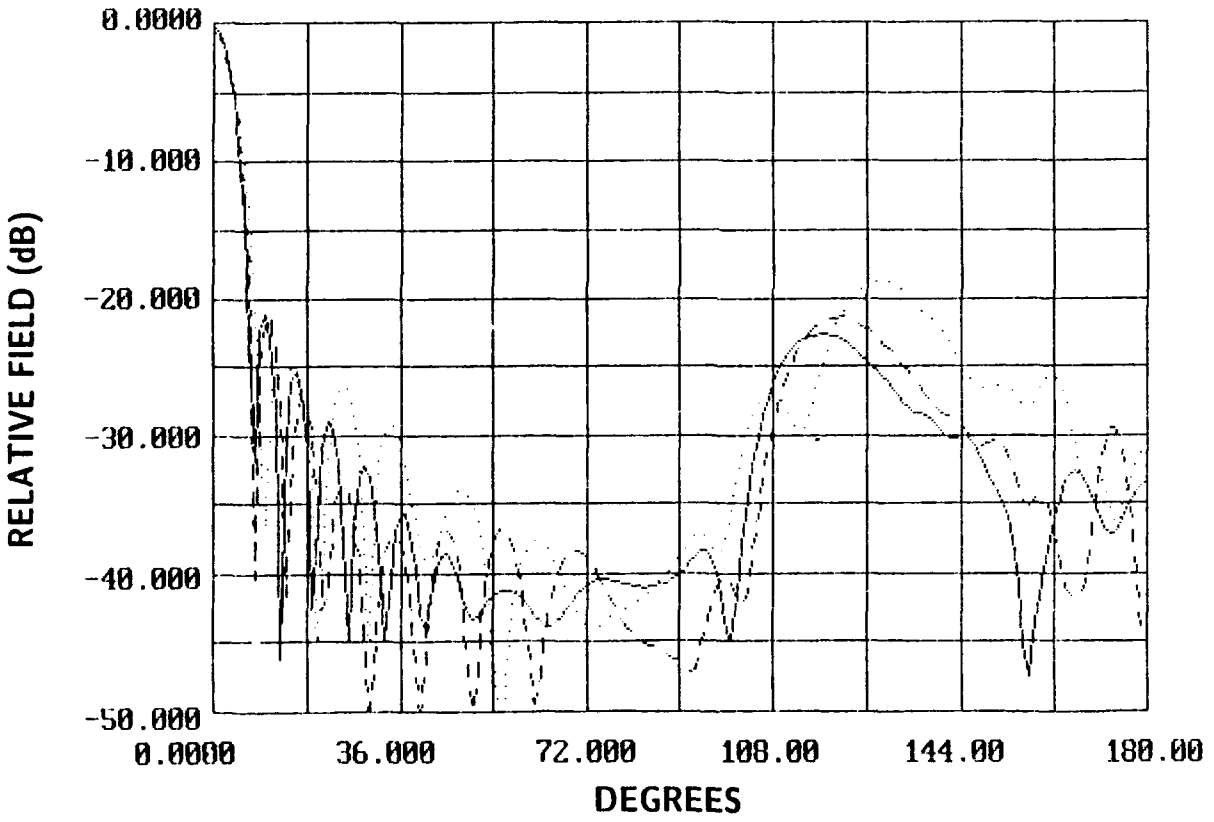

Figure 5.6 Antenna patterns of a two-dimensional parabolic reflectors having a diameter of 10λ and a focal length of 5λ and a constant resistive load η=1.0.The feed pattern is given by (5-1). —0.5λ from the edge, ---1.0λ from the edge, ···2.0λ from the edge.

at distances of 0.5λ, 1.0λ, and 2.0λ away from the edges. This figure shows that the wider the edge load, the higher the sidelobe levels and the lower the gain. Also, the sidelobe spacing increases as the width of the load increases, because the aperture appears to be smaller. The edge loads do somewhat lower the sidelobe level of the antenna but allow more energy to transmit through the antenna causing a larger spill-over lobe.

Tapering the edge loads lowers the sidelobes more effectively than the constant edge loads. The tapered loads have a much smaller lobe transmitted through the reflector than the constant edge loads and have a larger gain. Table I documents the relative levels of the main beams for various resistive tapers. Comparing Figures 5.7 and 5.8 with Figures 5.3 and 5.4 and examining the data in Table I leads to the conclusions that a quadratic resistive taper having an edge value equal to the constant resistive load produces lower antenna sidelobes and has higher gain. Thus, the tapered resistive loads provide better antenna performance than the constant resistive loads.

A heavy resistive taper produces lower sidelobes and a lower gain than a light resistive taper (Figure 5.7). Extending the resistive taper from 1λ to 2λ lowers the gain of the antenna and increases the lobe transmitted through the antenna but produces no significant changes to the sidelobe level (Figure 5.8).

TABLE I

Comparison of antenna patterns for reflector antennas with resistive loads.

RESISTIVE TAPER	MAINLOBE (Dbλ)	FIGURE
perfectly conducting	0.0	5.1
$\eta = 1.0$	-9.4	5.2
$\eta = 0.5\left(\frac{d}{D/2}\right)^2$	-1.6	5.3
$\eta = 2.0\left(\frac{d}{D/2}\right)^2$	-4.2	5.4
$\eta = 0.5$ at 0.5λ from edges	-0.2	-
$\eta = 0.5$ at 1.0λ from edges	-0.4	5.5
$\eta = 0.5$ at 2.0λ from edges	-1.2	-
$\eta = 1.0$ at 0.5λ from edges	-0.3	5.6
$\eta = 1.0$ at 1.0λ from edges	-0.6	5.6
$\eta = 1.0$ at 2.0λ from edges	-1.6	5.6
$\eta = 2.0$ at 0.5λ from edges	-0.3	-
$\eta = 2.0$ at 1.0λ from edges	-0.7	5.5
$\eta = 2.0$ at 0.5λ from edges	-2.0	-
$\eta = 0.5x^2$ at 1.0λ from edges	-0.1	5.7
$\eta = 1.0x^2$ at 1.0λ from edges	-0.2	5.7
$\eta = 2.0x^2$ at 1.0λ from edges	-0.2	5.7
$\eta = 0.5x^2$ at 2.0λ from edges	-0.2	5.8
$\eta = 1.0x^2$ at 2.0λ from edges	-0.3	5.8

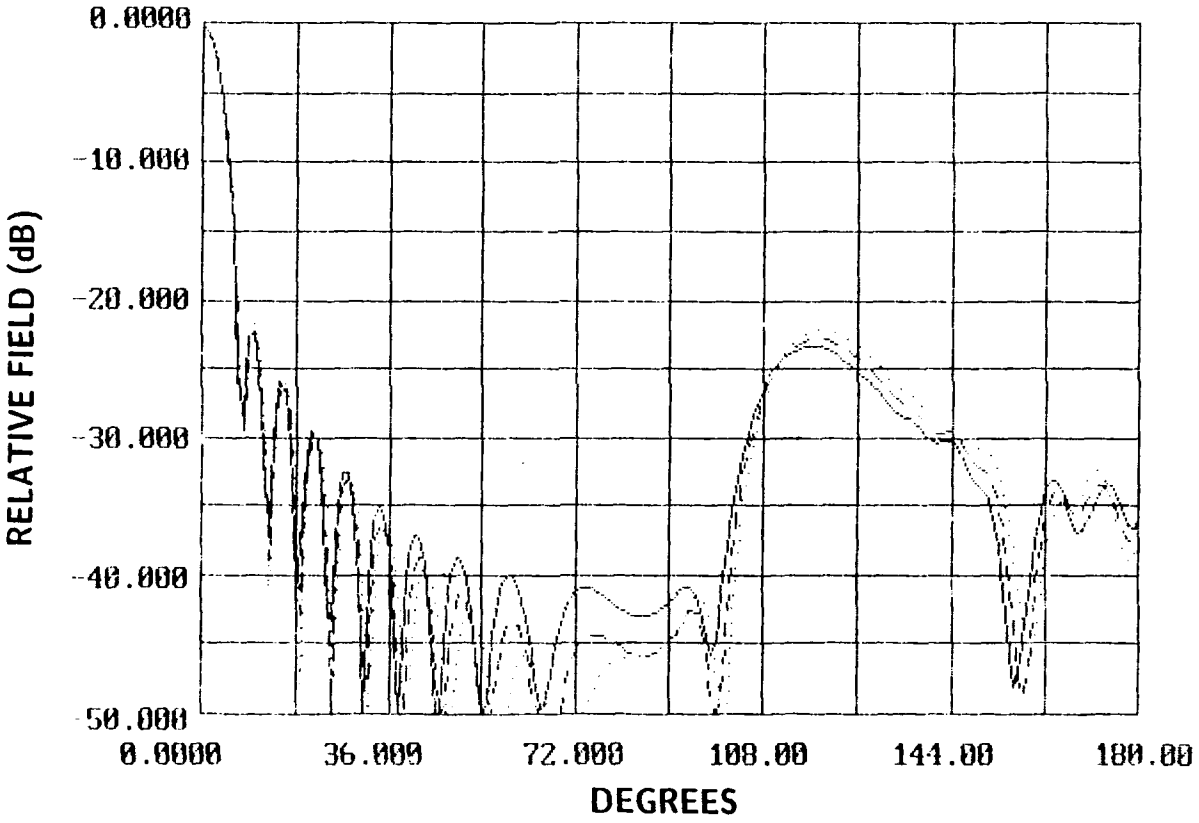

Figure 5.7 Antenna patterns of a two-dimensional parabolic reflectors having a diameter of 10λ and a focal length of 5λ and a quadratic resistive taper 1.0λ from the edges. The feed pattern is given by (5-1). — η_{max}=0.5, --- η_{max}=1.0, ··· η_{max}=2.0.

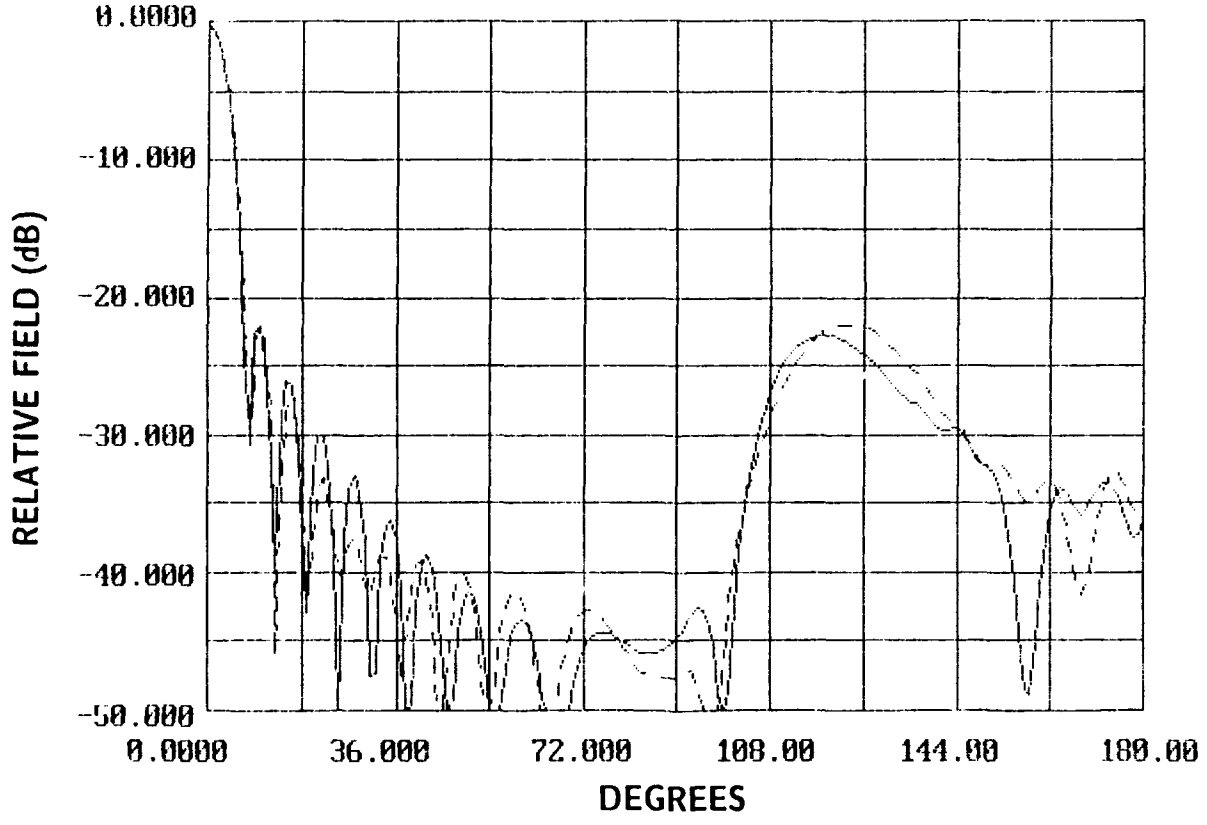

Figure 5.8 Antenna patterns of a two-dimensional parabolic reflectors having a diameter of 10λ and a focal length of 5λ and a quadratic resistive taper at the edges with η_{max}=1.0. The feed pattern is given by (5-1). — 1.0λ from the edge, ---2.0λ from the edge.

6. CONCLUSIONS

The scattering and antenna patterns of reflector antennas are modified by making part of the reflector from resistive materials. A perfectly conducting reflector has large backscattering lobes centered at 0° and 180°. The corresponding antenna pattern has a main lobe at 0° due to the focusing of the energy from the feed and a large sidelobe at 112° due to spillover from the feed. The goal of this research is to reduce the large scattering lobes while maintaining low sidelobes and a large gain.

The large backscattering lobes at 0° and 180° can be reduced by making the entire reflector resistive, but the gain of the antenna is also substantially reduced. Tapering the resistivity makes the backscattering main lobes narrower and lowers the sidelobes, but does not reduce the returns at 0° and 180°. The tapers do significantly reduce the sidelobes in the antenna pattern with a small reduction in the gain. Edge loads reduce the backscattering sidelobes and the antenna pattern sidelobes, but do not alter the main lobes.

In general, tapering the resistivity on the reflector surface provides a much better antenna pattern than a perfectly conducting reflector or a reflector with constant resistive loads. Adding a resistive taper also reduces the scattering sidelobes and the width of the scattering main lobes. The peaks of the scattering main lobes are not reduced through resistive tapers, though.

Future research in this area includes

1. Synthesis of resistive tapers that produce desired antenna sidelobe levels.
2. Synthesis of resistive tapers that produce desired scattering sidelobe levels.
3. Resistive tapers that reduce the backscattering main lobes while maintaining a respectable antenna pattern.

REFERENCES

1. J. D. Kraus, **Antennas**, McGraw-Hill, New York, 1988.

2. Y. T. Lo and S. W. Lee, ed., **Antennas**, Van Nostrand Reinhold Company, New York, 1988.

3. R. F. Harrington and J. R. Mautz, "An impedance sheet approximation for thin dielectric shells," IEEE Trans. Ant. Prop., Vol. AP-20, No. 5, Jul 1975, pp. 531-534.

4. R. F. Harrington, **Field Computation by Moment Methods**, Robert E. Krieger Publishing Co., Malabar, Florida, 1968.

5. M. Abramowitz and I. A. Stegen, Handbook of Mathematical Functions, Dover Publications, Inc., New York, 1972.

MISSION
of
Rome Air Development Center

RADC plans and executes research, development, test and selected acquisition programs in support of Command, Control, Communications and Intelligence (C^3I) activities. Technical and engineering support within areas of competence is provided to ESD Program Offices (POs) and other ESD elements to perform effective acquisition of C^3I systems. The areas of technical competence incluae communications, command and control, battle management information processing, surveillance sensors, intelligence data collection and handling, solid state sciences, electromagnetics, and propagation, and electronic reliability/maintainability and compatibility.